Journal of Cytology and Genetics 2025 VOL. **26** (NS): 27−34

RESEARCH ARTICLE

KARYOMORPHOLOGICAL STUDY OF *ZAMIOCULCAS ZAMIIFOLIA* (LODD.) ENGLER

CINTHYA CHRISTOPHER[1]*, D. G. SMITHA[2], J. M. ATHIRA[3], K. K. NISHA[1] AND T. J. SHAINA[1]

[1]Department of Botany, All Saints' College, University of Kerala, Thiruvananthapuram 695 007

[2]Department of Botany, University College, University of Kerala, Thiruvananthapuram 695 034

[3]Department of Botany, Christian College, University of Kerala, Thiruvananthapuram 695 572

* For correspondence. Email: cinthya_wilfred@yahoo.com

(Received 10 June 2025, revised accepted 12 August 2025)

SUMMARY *Zamioculcas zamiifolia* (Araceae), an unusually drought resistant medicinal plant is native to tropical East Africa, and subtropical southeast Africa. In the present study, its karyomorphology was investigated. The diploid chromosome number is 34. The karyotype consists of 7 pairs of chromosomes with median centromeres, 8 pairs of chromosomes with submedian centromeres and 2 pairs of chromosomes with subterminal centromeres. The karyotype formula is K = 2n = 34 = 4 Am + 4 Bm +4 Bsm + 2 Bst + 6 Cm + 12 Csm + 2 Cst. The average chromosome length is 7.08 µm and the total form per cent is 37.43. Based on karyotype asymmetry and degree of difference between the largest and smallest chromosomes of the complement and the position of centromere, the karyotype category of the species falls under 2A.

Keywords: *Zamioculcas zamiifolia,* Araceae, karyotype, idiogram.

INTRODUCTION

Zamioculcas zamiifolia, an unusually drought resistant medicinal plant belongs to the family Araceae, It is commonly known as "Zanzibar gem", "Zuzu plant" or emerald palm. It is a tropical perennial plant native to eastern Africa, from Kenya South to northeastern South Africa. The plant is grown in dry grassland and often on stony ground and has several fleshy stalks bearing alternate pinnate leaflets. It is an evergreen herb with a short, very thick rhizome. The leaflets have the capacity to sprout new plants and form tiny rhizomes at their base.

Z. zamiifolia is grown as an ornamental plant, mainly for its attractive glossy foliage. The ability of *Z. zamiifolia* to grow under low light condition, its tolerance to drought stress, its unique appearance, its low maintenance requirements and limited pest problems are characteristics that contribute significantly to its ornamental and landscaping value (Chen & Henny 2003). Cytologically, this is a little known species, and the earliest chromosome report of the species is by Jones (1957) who reported 2n = 34. Although the chromosome number of the species has been reported, karyotype analysis has not been undertaken so far. The study of morphology of

chromosomes has gained a new sphere of usefulness as an ally of taxonomy, phylogeny and evolution. The chromosomes being carriers of the genetic material, changes in them bear a direct relationship to the genetic-evolutionary processes at work, than do any other types of changes (Stebbins 1950). The role of karyotype analysis in solving major problems of taxonomy e.g. occurrence of the same chromosome number in different species of the same genus and the same number also observed in different genera as well. In such cases, the karyotypes of different taxa differ only in structural configurations.

In this backdrop, a karyomorphological investigation of *Z. zamiifolia* is significant and assumes importance. The major objectives of the study are twofold: (1) Collection, identification and cultivation of the species and (2) Karyotype analysis and idiogram construction.

MATERIAL AND METHODS

Field surveys were conducted to locate populations of *Z. zamiifolia* occurring in Thiruvananthapuram district of Kerala. Wild populations of the species were located and samples were collected from the Museum Campus, Thiruvananthapuram and Jawaharlal Nehru Tropical Botanic Garden and Research Institute, Palode. The collected samples were planted in the Field Gene Bank of All Saints' College. Somatic chromosome studies were made from root tip cells. The potted plants kept in the net house were watered well and exposed to bright sunlight for 2 h before collecting root tips from them. Young root tips were collected between 11.30 a.m. and 12.30 p.m. and pretreated with 0.002 M solution of 8-hydroxyquinoline (Tjio & Levan 1950) for 2 h at 4^0 C. The pretreated roots were washed well in tap water and fixed in Carnoy's fluid (3:1 absolute alcohol and glacial acetic acid). The fixation period of 2–4 d was found to yield good results. One or 2 meristematic tips were squashed on a slide using 2% acetocarmine. After putting on a cover glass, the slide is gently heated and pressed uniformly in the folds of a blotting paper. Mitotic metaphase was illustrated with photomicrographs, taken using Leica ICC 50 HD camera, attached to Leica DM 500 trinocular microscope. For karyotype analysis, average measurements of 3 somatic plates each from magnified (x 3000) prints were used. Photo-idiograms were prepared from photomicrographs, arranging them in descending order of their length and matching on the basis of their position of centromere. Values of measurements such as length of long arm (LA), length of short arm (SA), total chromosome length (TCL), arm ratio (r value), relative chromosomal length (RCL) and average chromosome length (ACL) were tabulated. Classifications of chromosomes were made following the systems proposed by Levan et al. (1964) in which the absolute median position of centromere (r = 1) are designated as M-type; those with arm ratios between 1 and 1.7 as m-type; arm ratios between 1.7 and 3.0 as sm-type; arm ratios between 3.0 and 7 as st-type and those with arm ratios exceeding 7 as t-type. Categorization of karyotype asymmetry was determined following Stebbins (1985). The total form per cent (TF%) was compu-

ted by the total short arm length of the chromosomes x 100. For constructing the karyotype formula, the chromosome lengths of the species was classified under 3 classes such as A = 9–11 µm, B = 7–9 µm and C = 5–7 µm. Idiogram was constructed based on the data elucidated.

OBSERVATIONS

The somatic complement consists of 34 chromosomes (Fig.1). The chromosomes of the complement were medium-sized. The details of measurements of chromosomes are given in Table 1. The chromosome length varied from 5.65 to 10.87 µm, the length of long arm varied between 3.05 and 6.09 µm and the length of short arm ranges from 1.52 to 5.0 µm, the arm ratio varies from 1.07 to 3.14 and the relative chromosome length varied from 4.70 to 9.03. The pattern of variation of TCL, r-value and RCL in the 17 chromosome pairs were estimated and depicted graphically (Figs 1, 2)

The karyotype consists of 7 pairs of median (m) type, 8 pairs of submedian (sm) type and 2 pairs of subterminal (st) type. For constructing karyotype formula, the chromosome lengths were grouped under 3 classes such as A = 9–11 µm, B = 7–9 µm and C = 5–7 µm, and accordingly the karyotype formula is K = 2n = 34 = 4 Am + 4 Bm + 4 Bsm + 2 Bst + 6 Cm + 12 Csm + 2 Cst. The ACL is 7.08 µm and the TF% is 37.43. Based on karyotype asymmetry and both degrees of difference between the largest and smallest chromosome of the complement and the position of centromere *Z. zamiifolia* falls into 2A category. Idiogram was also

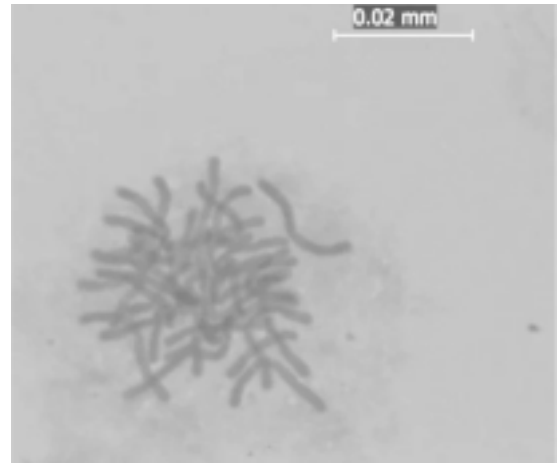

Fig. 1: *Z. zamiifolia*. Somatic chromosomes.

TABLE 1: Karyotype analysis of *Z. zamiifolia.*

Chrom. pair	Chromosome length in µm			r value	RCL	Chrom. type
	Long arm	Short arm	Total length			
1	5.87	5.00	10.87	1.17	9.03	m
2	5.00	4.13	9.13	1.21	7.58	m
3	5.65	3.05	8.70	1.85	7.22	sm
4	6.09	1.97	8.26	3.09	6.86	st
5	4.13	3.69	7.82	1.12	6.50	m
6	5.00	2.39	7.39	2.09	6.14	sm
7	3.70	3.47	7.17	1.07	5.96	m
8	4.57	1.95	6.52	2.34	5.42	sm
9	4.26	2.26	6.52	1.88	5.42	sm
10	3.91	2.39	6.30	1.64	5.23	m
11	4.78	1.52	6.30	3.14	5.23	st
12	4.35	1.95	6.30	2.23	5.23	sm
13	3.26	2.83	6.09	1.15	5.06	m
14	3.05	2.82	5.87	1.08	4.88	m
15	3.91	1.96	5.87	1.99	4.88	sm
16	3.91	1.74	5.65	2.24	4.70	sm
17	3.70	1.95	5.65	1.90	4.70	sm

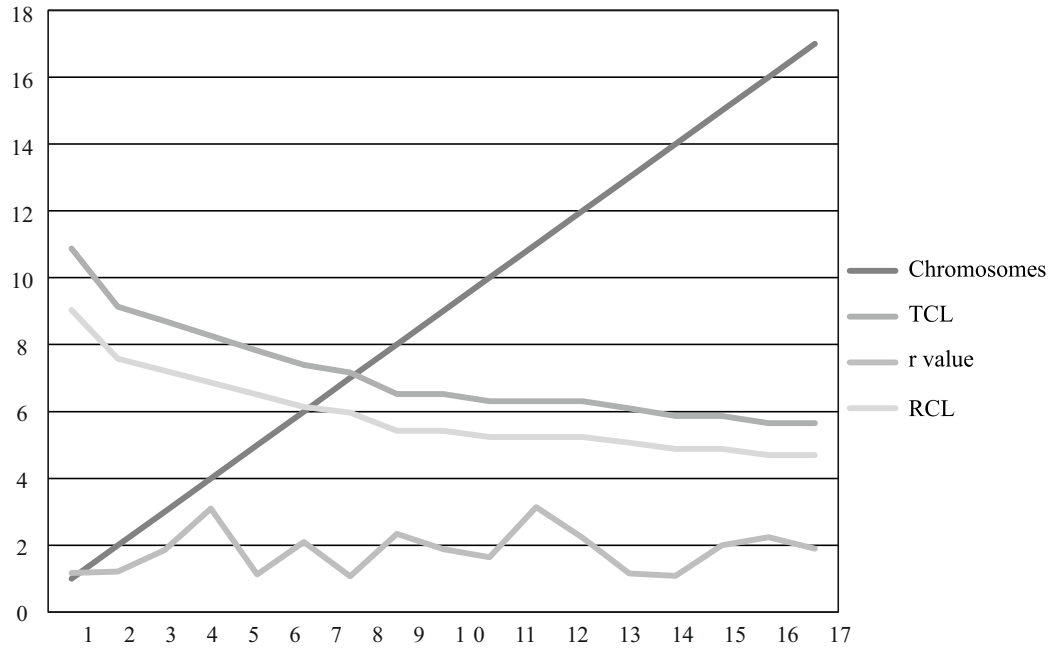

Fig. 2: *Z. zamiifolia***.** Pattern of variation of TCL, r-value and RCL in 17 chromosome pairs.

constructed based on chromosome data and the karyotype in this species is found to be moderately asymmetrical (Fig. 3).

DISCUSSION

Cytological characters, such as chromosome number and karyomorphology have been considered as reliable guides in studies of taxonomic and evolutionary relationships.

Karyotype analysis has been extensively carried out in plant phylogenetic and diversity studies for more than a hundred years. In this era of modern molecular techniques, cytology is still a valuable tool for taxonomy, phylogeny and diversity studies. The information like chromosome number, size and morphology has been of considerable value in understanding interrelations and delimitation of taxa. Cytotaxonomic, chromosome architecture and its behaviour are blueprints to adopt proper strategy for the genetic improvement of the plant species. Several workers have done cytogenetic studies particularly chromosome number and morphology at mitotic division and, chromosomal association and behaviour during meiotic division in the members of the family Araceae.

The chromosomes, being the carriers of the genetic material, changes in them, both numerical and structural, bear direct relationship to the genetic-evolutionary processes than do any other changes (Stebbins 1971). The karyomorphological information can help understand the systematic relationships of plants at different taxonomic levels.

The factor of basic chromosome number at

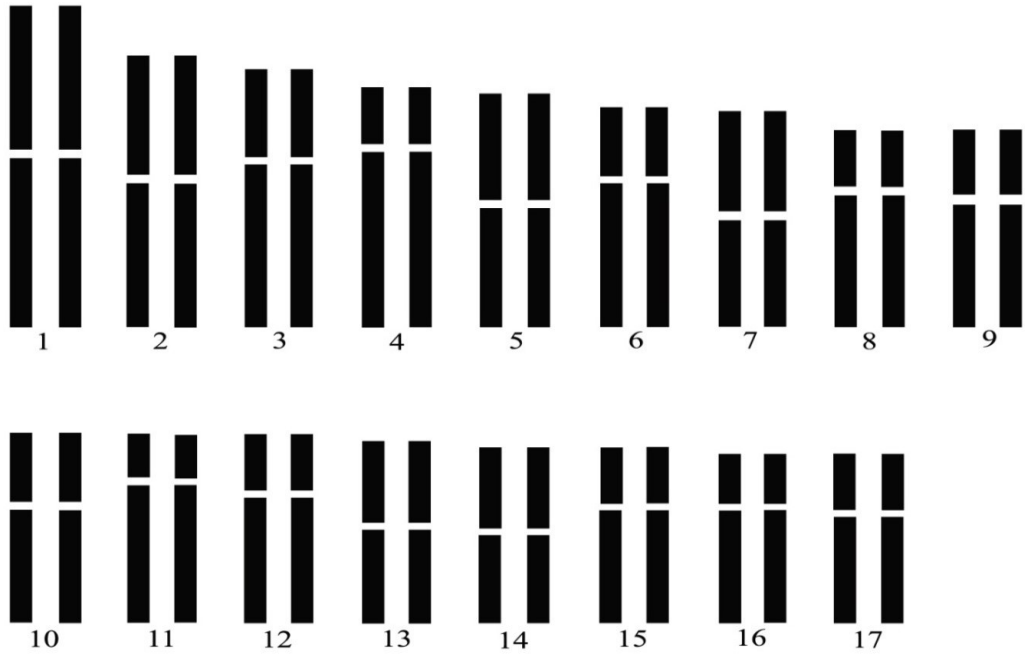

Fig. 3: *Z. zamiifolia*. Idiogram.

various taxonomic levels has played a vital role in shaping the prevailing concept of evolution in plants, and this has formed one of the major criteria considered for formulating phylogenetic speculations. It also serves as a reliable and stable marker of the direction of evolution. Diminution of basic chromosome numbers, rather than their increase, often occurs playing significant role in chromosome evolution (Stebbins 1971). Since the somatic chromosome number in the present taxon is 34, it can be construed that the species and genus are x = 17 basic. But, according to Stebbins (1971), this is too high a basic number to be considered as the original. His contention is that basic numbers of the order x = 9 and 10 could be secondary ones derived from low ancestral ones. The earlier works in Araceae (Jones 1957, Larsen 1969, Marchant 1973, Peterson 1989) have proposed x = 14 or 12 as the earlier evolved basic constitutions in the family Araceae derived from a primary x = 7. But the present x = 17 in the species does not conform to any of the x = 14 or 12, proposed earlier numbers; and hence the ancestral constitution of the x = 17 must be some other lower ones. There can be 2 possibilities for the origin of x = 17 such as (1) x = 9 by polyploidy as this followed by descending aneuploidy (9 x 2 = 18 – 1), resulting in x = 17. According to this postulation, the x = 17 in the present taxon could be a tertiary state of polyploidy origin (2) an alternative possibility is that an x = 17 derived by secondary hybrid polyploidy involving 2 ancestral taxa with x = 9 and 8 (9 + 8 = 17). In either

case, the 2n = 34 present in the species could be of polyploid origin.

Polyploidy is the most widespread cytogenetic process that has contributed to species formation and evolution in plants. This is mainly due to the ability of polyploids to increase the chances of fertilization by breaking reproductive barriers and also their higher tolerance to adverse environmental conditions (Stebbins 1971). Aspects such as types of polyploids, modes of their origin and development, cytogenetic behaviour and significance in speciation and evolution have been discussed and reviewed by many cytologists (Clausen et al. 1945, Darlington 1956, Stebbins 1971, Harlan & De Wet 1975). According to an estimate by Love (1963), incidence of polyploidy is about 30 per cent in the dicotyledons, 50 per cent in the monocotyledons and still higher percentage in the pteridophytes. In angiosperms, aneuploidy is known to occur most often at the diploid level (Stebbins 1971). In the best known examples this phenomenon involves an increase or decrease of one chromosome at a time brought about by various karyological mechanisms such as unequal translocation between nonhomologous chromosomes, fragmentation of centric fragments, unequal separation of chromosomes into daughter cells during mitosis and by nondisjunction of bivalents during meiosis (Stebbins 1971). According to Stebbins (1950), progressive aneuploid increase of basic numbers occurs less frequently in angiosperms. It is also reported earlier that the variation in chromosome number may be due to aneuploid changes at the diploid level followed by polyploidy or aneuploidy at the polyploid level in the family Araceae (Mayo et al. 1997)

The study of morphology of chromosomes has gained a new sphere of usefulness as an ally of taxonomy, phylogeny and evolution. Stebbins (1971) described 6 different karyotype characteristics which can be observed and compared such as (1) differences in the absolute chromosome size, (2) differences in the position of centromere, (3) differences in relative chromosome size, (4) differences in basic number, (5) number and position of satellites and (6) degree and distribution of heterochromatin.

The size and shape of the chromosomes are also quite variable in the family Araceae. Chromosome length varies from 1–17 µm depending on the genus. The chromosomes have been observed to differ greatly in size and shape within a single genome in certain cases (Mayo et al. 1997). In the present study, the TCL varied from 5.65 to 10.87 µm.

The length of long arm varied from 3.05 to 6.09 µm, length of short arm varies from 1.52 to 5.0 µm, total length of each chromosome varied from 5.65 to 10.87 µm. In the present species, the arm ratio ranged from 1.07 to 3.14. The karyotype was composed of 7 pairs of m-type, 8 pairs of sm-type and 2 pairs of st-type. The formula for the karyotype is K = 2n = 34 = 4 Am + 4 Bm +4 Bsm + 2 Bst + 6 Cm + 12 Csm + 2 Cst.

The RCL, which is the percentage of actual length of chromosome to the total length of

chromosome of the species varied from 4.70 to 9.03. The ACL, which is the ratio of total chromosome length to the haploid number of the species is calculated as 7.08 μm.

TF% which is the percentage of total short arm length to the total length of chromosome is a parameter which reveals the asymmetry level of the karyotype. The TF% value varies from 0 to 50 in the genomes. In the present study, the TF% was estimated to be 37.43 which reveals that the karyotype is marginally or moderately asymmetrical.

The concept of karyotype symmetry verses asymmetry was developed by the Russian School of comparative morphology of the karyotype led by Levitzky (1931). Karyotype with chromosomes which are mostly of the same size and having median centromeres are considered to be symmetrical and those with appreciable difference in size of chromosomes and increased frequency of subtelocentric chromosomes are considered asymmetrical. The information about karyotype asymmetry has been known to be significant in many plant taxa where associations occur between increasing asymmetry of the karyotype and other characteristics such as chromosome number, plant morphology or plant habit. In order to facilitate an effective study of such associations, Stebbins (1985) classified the karyotype asymmetry under 12 categories (1A−4C) taking into account both the degrees of difference between the largest and smallest chromosomes of the complement and the position of the centromere on the chromosome. According to him, increasing asymmetry occurs through incidence and establishment of pericentric inversions changing median centromere positions to subterminal ones. The first chromosome to be affected in the process is usually the satellite chromosome. He has also suggested that as a second step in the evolution of karyotype asymmetry, inversions are followed by unequal translocations resulting in intrakaryotypic size difference. The chromosome category based on karyotype asymmetry taking into account both degrees of difference between the largest and smallest chromosome of the complement and the position of centromere on the chromosome reveals that the present species is of 2A category.

The significance of detailed karyomorphological study is providing clues for the association of changes in chromosome both numerical and structural with plant morphological differences has been documented and brought out from the results of extensive karyotype studies carried out in araceous tuber crop, *Colocasia esculenta* (taro). This plant exists in India in a multiplicity of morphological types, and they are of 2 ploidy levels, diploids and triploids both having x = 7 basic. The study has brought out the existence of over 12 karyotypically distinct cytotypes among the Indian taros which differ from one another exceedingly in plant morphological characters. The karyotype repatterning resulting in the different cytotypes involved chromosome structural repatterning in several chromosomes, particularly 3 marker

chromosomes, 1, 3 and 9. The study brought out the karyomorphological basis of the degree and spectrum of plant morphological difference evident in the species complex (Sreekumari & Mathew 1991, 1995, Sreekumari et al. 2010). Similar findings highlighting the significance of karyomorphological studies elucidating systematic issues have been known in other plant groups like gymnosperms and angiosperm families, Liliaceae, Rubiaceae etc. (Mathew & Christopher 2018a, 2018b, 2019).

REFERENCES

CHEN J & HENNY R J 2003 Z Z A unique tropical ornamental foliage plant *Hort Technol* **13** 458−462

CLAUSEN J, KECK D D & HIESEY W N 1945 Experimental studies on the nature of species II Plant evolution through amphiploidy and autoploidy with examples of Madiinae *Carnigie Inst Washinton Publ* 564

DARLINGTON C D 1956 *Chromosome botany* George Allen & Unwin London

HARLAN J R & DE WET J M J 1975 The origins of polyploidy *Bot Rev* **41** 361−390

JONES G E 1957 *Chromosome numbers and phylogenetic relationships in the Araceae* Ph D Thesis University of Virginia

LARSEN K 1969 Cytology of vascular plants: III A study of Thai Aroids *Dansk Botanisk Arkiv* **27** 39−59

LEVAN A, FREDGA K & SANDBERG A A 1964 Nomenclature for centromeric position on chromosomes *Hereditas* **52** 201−220

LEVITZKY G A 1931 The "Karyotype" in systematics *Bull Appl Bot Genet Pl Br* **27** 187−240

LOVE A 1963 The evolutionary framework of biological species concept *In* Genetics Today *Proc X International Congr Genet* **2** 409−415

MARCHANT C J 1973 Chromosome variation in *Araceae* V Acoreae to Lasieae *Kew Bull* **28** 199−210

MAYO S J, BOGNER J & BOYCE P J 1997 *The genera of Araceae* Royal Botanic Gardens Kew London

MATHEW P M & CHRISTOPHER C 2018a Cytology in the systematics phylogeny and evolution II – Gymnosperms *J Cytol Genet* **19** (NS) 63−69

MATHEW P M & CHRISTOPHER C 2018b Cytology in the systematics phylogeny and evolution III – Liliales *J Cytol Genet* **19** (NS) 71−81

MATHEW P M & CHRISTOPHER C 2019 Cytology in the systematics phylogeny and evolution IV – Rubiaceae *J Cytol Genet* **20** (NS) 1−11

PETERSEN G 1989 Cytology and systematics of *Araceae Nord J Bot* **9** 119−166

SREEKUMARI M T & MATHEW P M 1991 Karyomorphologically distinct morphotypes in taro (*Colocasia esculenta*(L) Scott) *Cytologia* **56** 399−402

SREEKUMARI M T & MATHEW P M 1995 Karyotype distinctions in Indian taros *J Cytol Genet* **30** 143−149

SREEKUMARI M T, MATHEW P M & NUSAIFA BEEVI R 2010 Phylogeny and cytological evolution of Indian taro *J Root Crops* **13** 172−176

STEBBINS G L 1950 *Variation and evolution in plants* Columbia University Press New York

STEBBINS G L 1971 *Chromosomal evolution in higher plants* Edward Arnold London

STEBBINS G L 1985 Polyploidy hybridization and the invasion of new habitats *Ann Mo Bot Gard* **72** 824−832

TJIO J H & LEVAN A 1950 The use of oxyquinoline in chromosome analysis *Ann Est Exp de Aula De* **2** 21−64

Journal of Cytology and Genetics 2025 VOL. **26** (NS): 35−47

RESEARCH ARTICLE

SYNTHESIS OF SILVER NANOPARTICLES FROM *PAMBURUS MISSIONIS*: A NOVEL APPROACH FOR MOSQUITO CONTROL AND POLLUTANT DEGRADATION**

M. SAI YASWANTHI*, R. B. ACHYUTH BABU, S. ANKANNA AND N. SAVITHRAMMA
Department of Botany, Sri Venkateswara University, Tirupati 517 502, India
*For correspondence. Email: drsaiyaswanthi2812@gmail.com

(Received 27 September 2025, revised accepted 18 October 2025)

SUMMARY This study explores the biosynthesis of silver nanoparticles (AgNPs) using leaf and bark extracts of *Pamburus missionis* (Rutaceae), a medicinal plant, highlighting its potential in the context of plant biotechnology for environmental and human health. The AgNPs were synthesized using aqueous plant extracts and characterized through UV-Vis spectroscopy, FTIR, Dynamic light scattering (DLS), Zeta potential analysis, and Transmission Electron Microscopy (TEM). The resulting nanoparticles ranged in size from 1−150 nm, indicating their suitability for biological and catalytic applications. Larvicidal efficacy was evaluated against mosquito larvae at varying concentrations of 10−100 ppm, with significant mortality observed from 50 ppm onwards. Bark-derived AgNPs exhibited the highest larvicidal activity, achieving 95% mortality at 100 ppm (IC_{50} = 48.45 ppm, IC_{90} = 94.73 ppm), while leaf-derived AgNPs showed 91% mortality (IC_{50} = 42.88 ppm, IC_{90} = 98.14 ppm). In terms of environmental application, the AgNPs exhibited efficient photocatalytic degradation of methylene blue dye, with leaf-derived AgNPs achieving 85% degradation within 120 min, surpassing bark-derived AgNPs at 78%. These findings highlight the dual benefits of plant-derived nanomaterials in public health and environmental remediation, reinforcing the role of plant nanobiotechnology in addressing ecological challenges and promoting human well-being.

Keywords: Silver nanoparticles, *Pamburus missionis,* larvicidal activity, photocatalysis.

INTRODUCTION

Every year, millions of people worldwide suffer from mosquito-borne diseases such as malaria, dengue, chikungunya, and Zika (Naik et al. 2023). Despite the development of various chemical products to combat these vector-borne diseases, this conventional mosquito control strategies, which rely heavily on synthetic insecticides, have led to several drawbacks, including insecticide resistance, environmental contamination, and harmful effects

** Paper presented at the XV All India Conference on Cytology and Genetics held on 11th and 12th September 2025.

on non-target organisms (Onen et al. 2023, Saxena et al. 2016, Zargham et al. 2023). At the same time, rapid industrialization has resulted in the widespread release of synthetic dyes and organic pollutants into aquatic ecosystems (Piyawan et al. 2023). Among these, methylene blue is a commonly used dye that poses significant risks due to its persistence, toxicity, and resistance to biodegradation (Rania et al. 2022). Conventional wastewater treatment methods are often insufficient for its complete removal (Sadia et al. 2024). Furthermore, polluted water bodies often serve as breeding grounds for mosquitoes, thereby contributing to population growth and increasing the risk of mosquito-borne diseases (Benelli et al. 2016). These dual challenges—mosquito-borne diseases and environmental pollution—highlight the urgent need for safer, more sustainable, and eco-friendly alternatives. Developing cost-effective and environmentally compatible remediation strategies is therefore, essential for protecting both human health and ecological stability.

Green synthesis of nanoparticles has emerged as a promising approach in nanotechnology, offering an eco-friendly, cost-effective, and efficient method to address these dual challenges (Malik et al. 2023). Among various nanomaterials, silver nanoparticles (AgNPs) have attracted significant attention due to their broad spectrum of antimicrobial, larvicidal, and catalytic properties (Abbas et al. 2024, Okoye et al. 2022). Particularly, plant-mediated synthesis provides a simple one-pot method that utilizes phytochemicals as natural reducing and stabilizing agents. This approach eliminates the need for hazardous chemicals, high temperatures, or high pressures, thereby ensuring both environmental safety and scalability (Huq et al. 2022, Yugandhar et al. 2015). Many medicinal plants have been investigated for the synthesis of nanoparticles; however, several valuable yet underexplored species remain to be studied. *Pamburus missionis*, a medicinally important plant belonging to the Rutaceae, has so far remained unexplored in nanoparticle synthesis. Traditionally, it has been used to treat various ailments such as arthritis, rheumatism, paralysis and digestive disorders (Jayaweera 1982, Somasundaram 1967).

In this study, we report the eco-friendly synthesis of AgNPs using aqueous leaf and bark extracts of *P. missionis*. The synthesized nanoparticles were systematically characterized and evaluated for their dual functionality: (i) larvicidal activity against mosquito larvae and (ii) photocatalytic degradation of methylene blue dye.

MATERIAL AND METHODS

Leaves and bark of *P. missionis* were collected from Mamandur forest near Balupalle, Karakambadi Rural, Tirupati, Andhra Pradesh, India (GPS: 13°46'02.6"N; 79°26'02.5"E). The samples were thoroughly washed, shade-dried for 20 d, ground into fine powder, and stored for further use.

Aqueous extracts were obtained by boiling 5 g of dried plant powder in 100 ml of distilled water for 30 min, followed by incubation for 24 h and filtration through Whatman No.1 filter paper.

For AgNPs synthesis, 5 ml of plant extract was mixed with 50 ml of 1 mM $AgNO_3$ solution and heated at 60° C. The mixture was centrifuged at 10000 rpm for 20 min to collect purified nanoparticles (Venkateswarlu et al. 2010, Yugandhar et al. 2015). The formation and properties of AgNPs were analysed using UV-Vis spectroscopy (200–800 nm), Fourier Transform Infrared Spectroscopy (FTIR), Dynamic Light Scattering (DLS), Zeta potential, and Transmission Electron Microscopy (TEM).

Larvicidal activity was assessed by exposing mosquito larvae to different concentrations of AgNPs (10, 20, 30, 50, 80 and 100 ppm). Mortality was recorded, and lethal concentrations were determined (Bharathi & Suseem 2024, Mahalingam et al. 2023). Photocatalytic efficiency was tested using methylene blue dye degradation. A total of 10 mg of AgNPs was added to the dye solution (100 ml) and exposed to sunlight. Absorbance was measured at 664 nm using UV-Vis spectroscopy at intervals of 5, 15, 30, 60, 90 and 120 min (Rama et al. 2023, Yugandhar et al. 2019).

OBSERVATIONS

The addition of aqueous extracts to $AgNO_3$ solution produced a distinct colour change from yellowish-brown to dark-brown, confirming the successful synthesis of AgNPs (Figs 1, 2).

UV–Vis spectroscopy revealed strong surface plasmon resonance (SPR) peaks at 439 nm for leaf-derived AgNPs (PmL-AgNPs) (Fig. 3) and 429 nm for bark-mediated AgNPs (PmB-AgNPs) (Fig. 4), confirming nanoparticle formation. The slightly lower SPR value for bark suggests smaller average particle size compared to leaf extracts.

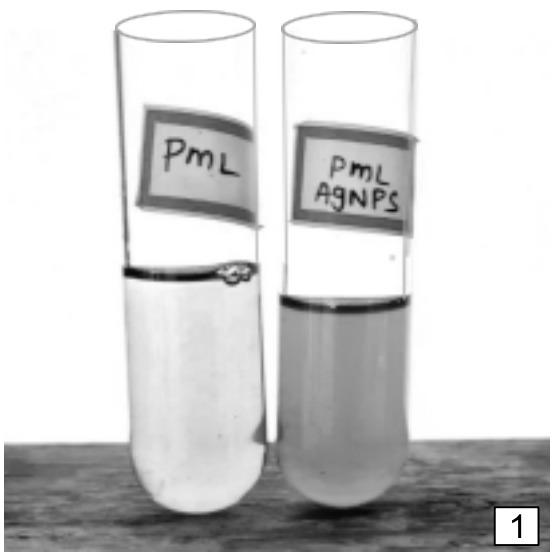

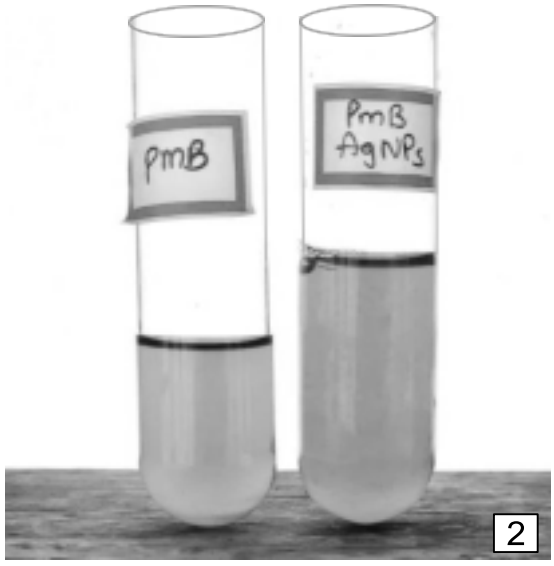

Figs 1 & 2: *P. missionis.* 1. AgNPs synthesis from leaf extract (PmL-AgNPs). 2. AgNPs synthesis from bark extract (PmB-AgNPs).

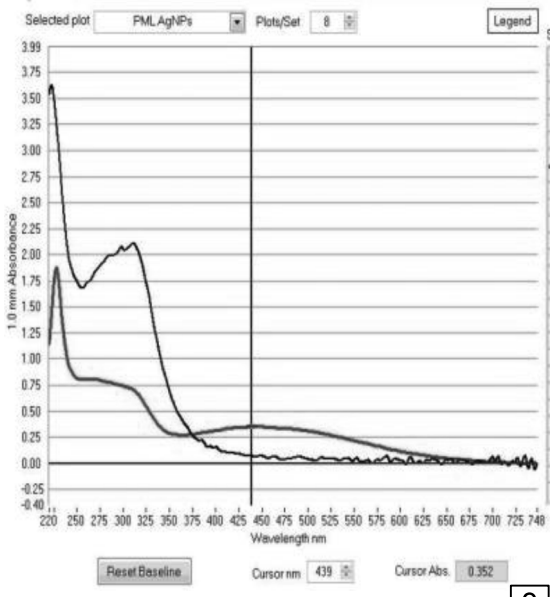

3

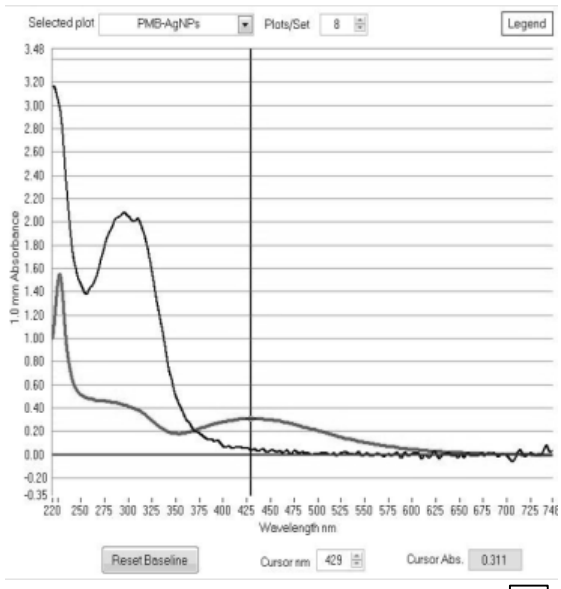

4

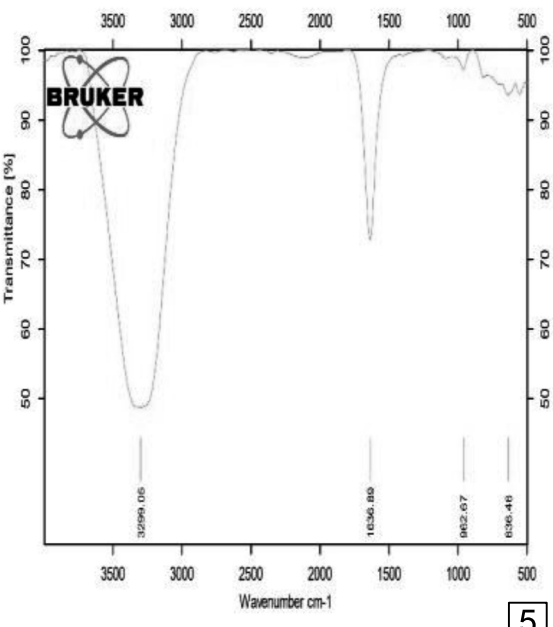

5

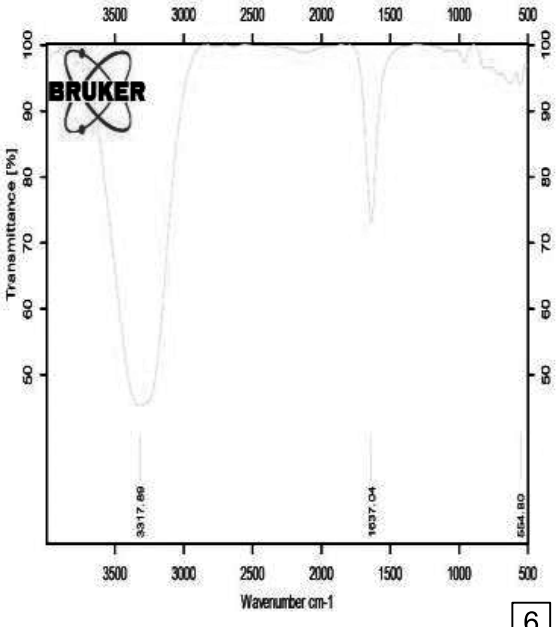

6

Figs 3–6: 3. UV-Vis peak of PmL-AgNPs at 439 nm. 4. UV-Vis peak of PmB-AgNPs at 429 nm. 5. FTIR peaks of extracts and synthesized AgNPs. 6. FTIR peaks of PmL-AgNPs.

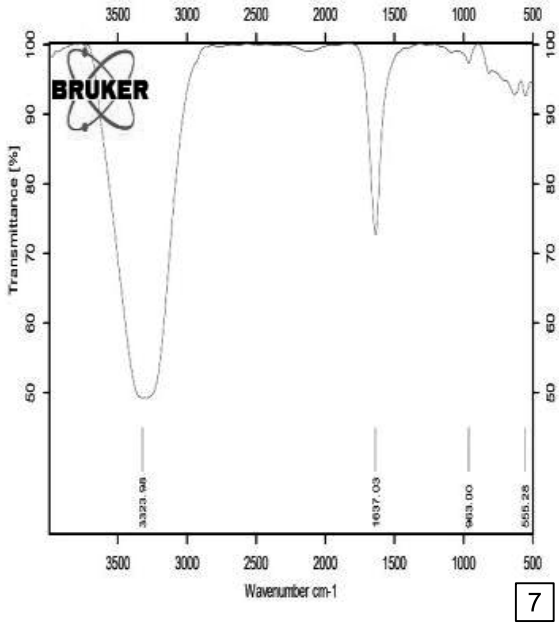

7

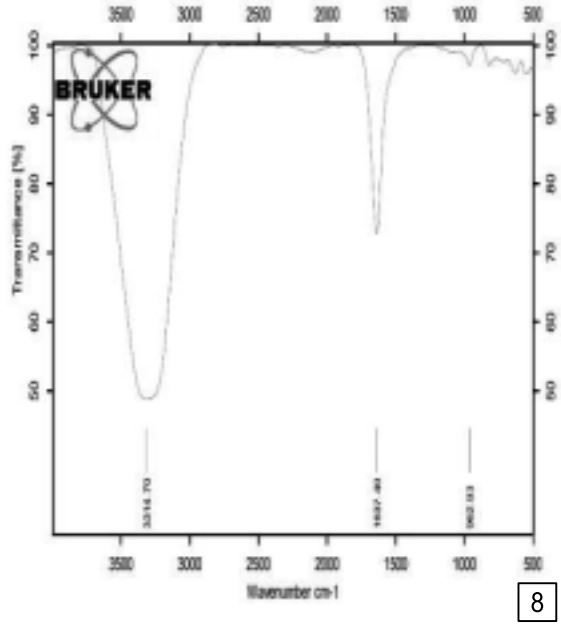

8

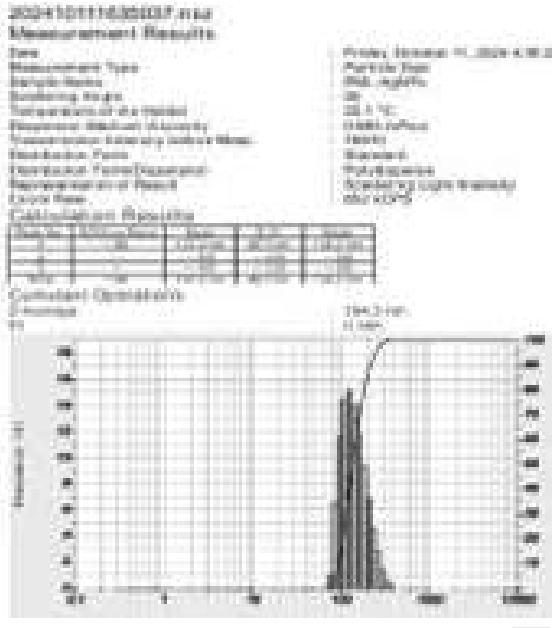

9

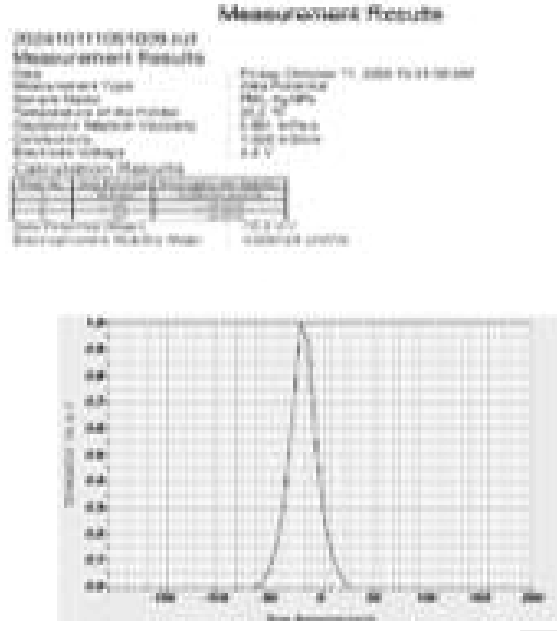

10

Figs 7–10: 7. FTIR peaks of bark extract of *P. missionis.* 8. FTIR peaks of PmB-AgNPs. 9. The size range of PmL-AgNPs from DLS (2–100 nm). 10. Surface charge of PmL-AgNPs from Z-potential (–15.9 mV).

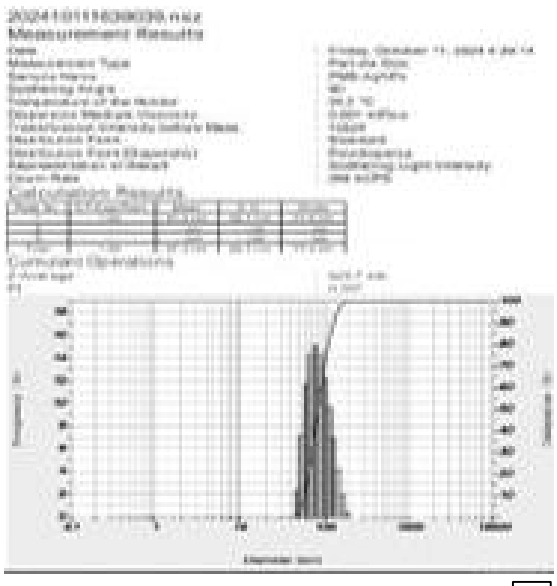

11

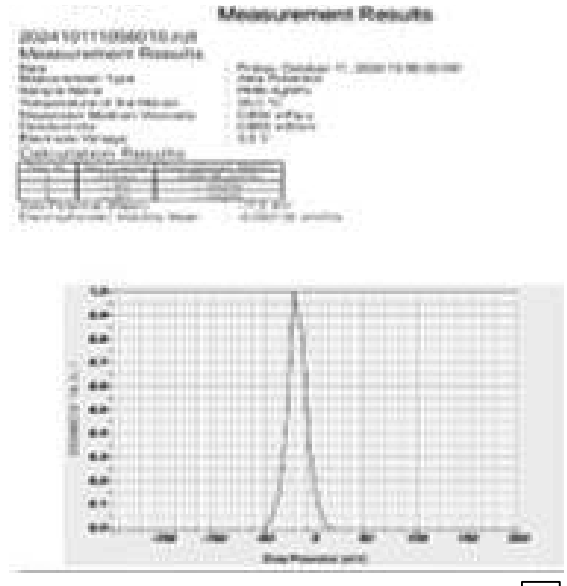

12

Figs 11 & 12: 11.The size range of PmB-AgNPs from DLS (40–200 nm). 12. Surface charge of PmB-AgNPs from Z-potential (–17.6 mV).

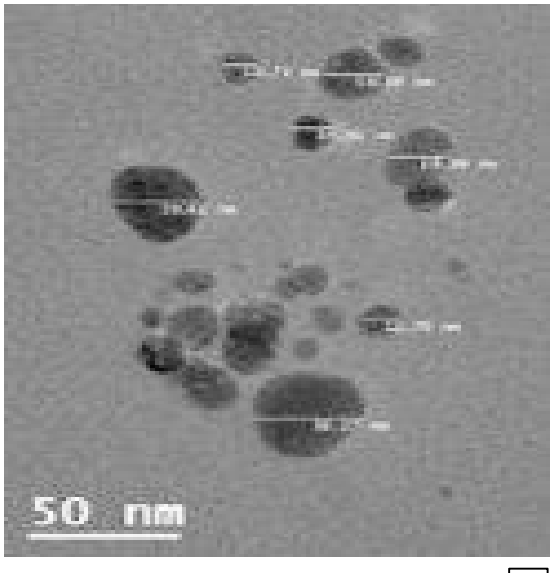

13

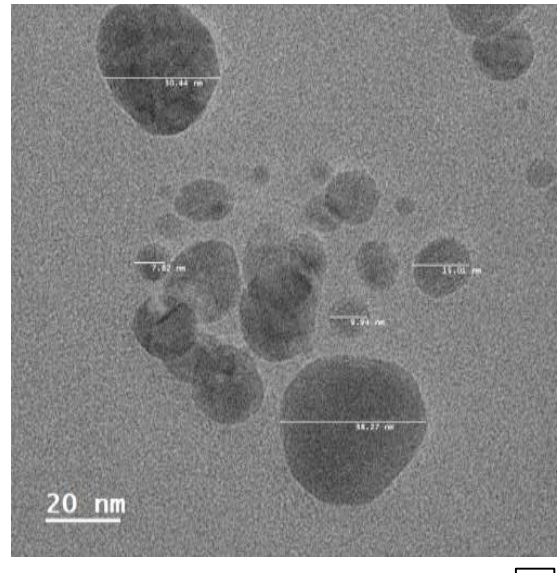

14

Figs 13 & 14: 13. TEM image of PmL-AgNPs at 50 nm magnification showing the sizes of AgNPs (10-40 nm). 14. TEM image of PmL-AgNPs at 20 nm magnification.

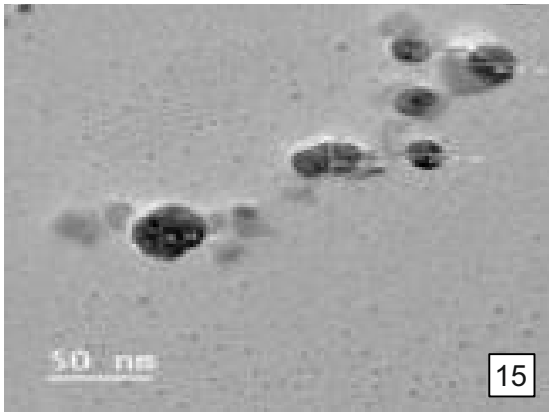

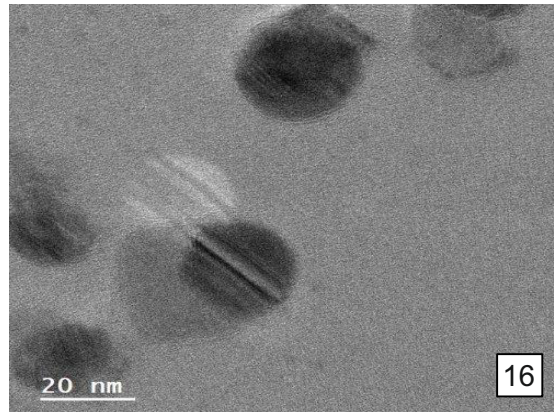

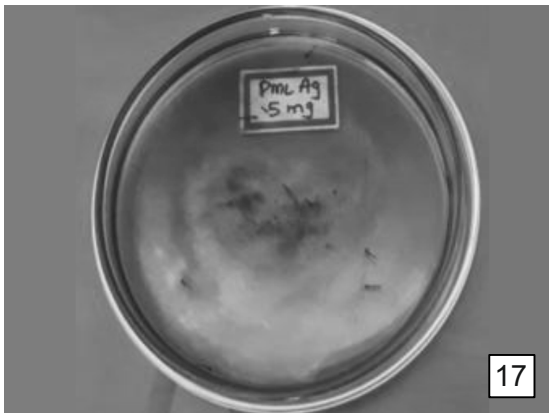

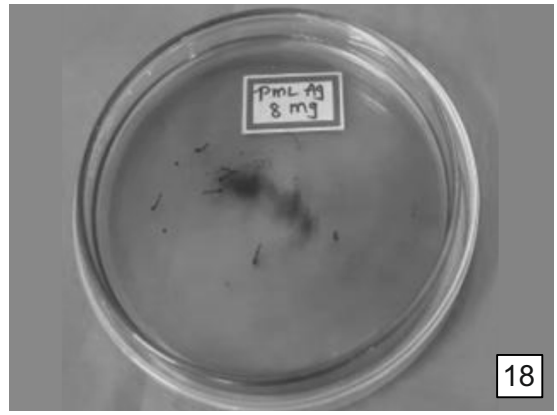

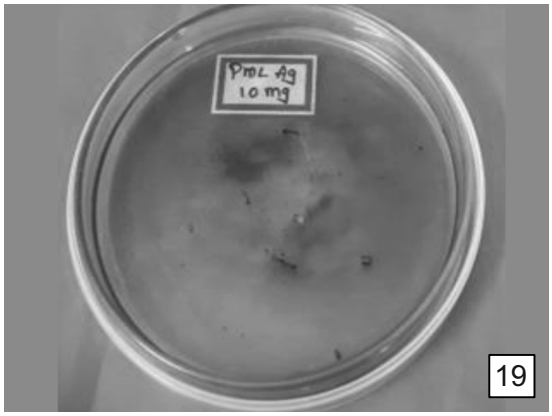

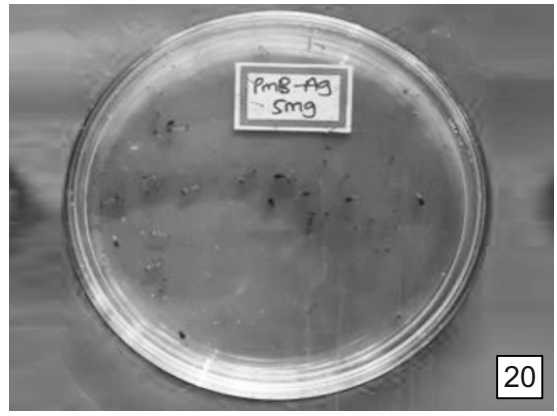

Figs 15–20: 15. TEM image of PmB-AgNPs at 50 nm magnification showing the sizes of AgNPs (10–30 nm). 16. TEM image of PmB-AgNPs at 20 nm magnification with clear fringes on the surface. 17. Larvae treated with 50 ppm concentration of PmL-AgNPs. 18. Larvae treated with 80 ppm concentration of PmL-AgNPs. 19. Larvae treated with 100 ppm concentration of PmL-AgNPs. 20. Larvae treated with 50 ppm concentration of PmB-AgNPs.

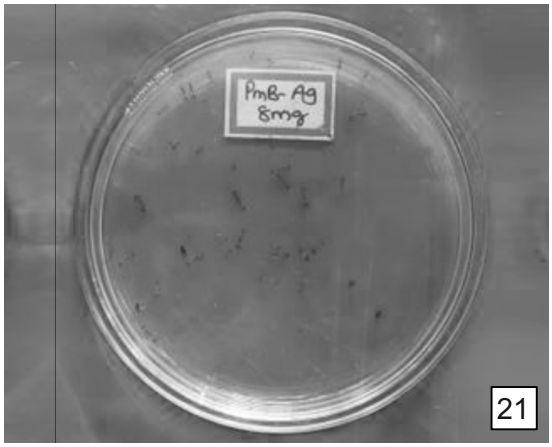

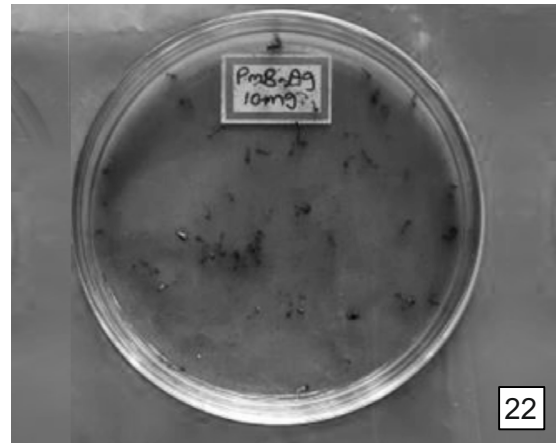

Figs 21 & 22: 21. Larvae treated with 80 ppm concentration of PmB-AgNPs. 22. Larvae treated with 100 ppm concentration of PmB-AgNPs.

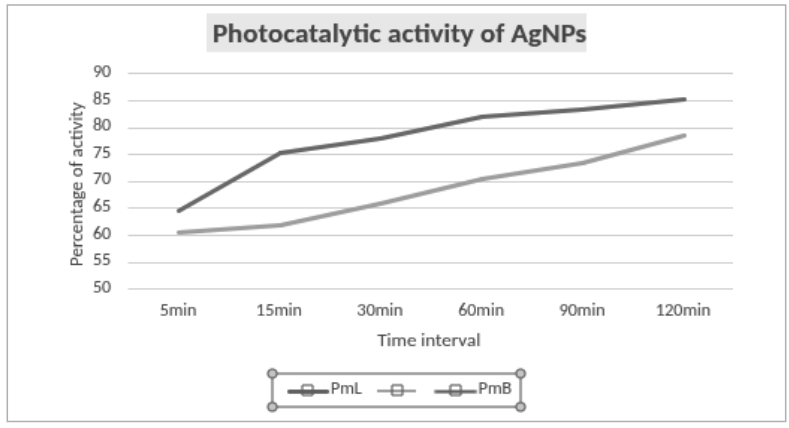

Fig. 23: Graph of photocatalytic activity of AgNPs from *P. missionis* in time interval of 5–120 min.

FTIR analysis confirmed the role of phytochemicals in reducing and stabilizing AgNPs. In the leaf extract, peaks were observed at 3299 cm^{-1} (carboxylic acids), 1636 cm^{-1} (C=C alkene), 962 cm^{-1} (N–H amine), and 636 cm^{-1} (halo group) (Fig. 5). After AgNP synthesis, the spectrum showed peaks at 3317 cm^{-1} (alcohol), 1637 cm^{-1} (alkene), and 554 cm^{-1} (halo group) (Fig. 6). Similarly, the bark extract exhibited peaks at 3323 cm^{-1} (alcohol), 1637 cm^{-1} (alkene), 963 cm^{-1} (amine), and 555 cm^{-1} (halo group) (Fig. 7), while the bark-derived AgNPs retained peaks at 3314 cm^{-1} (alcohol), 1637 cm^{-1} (alkene), and 962 cm^{-1} (amine) (Fig. 8). The slight shifts and disappearance of certain peaks in AgNPs compared to crude extracts confirm the binding of biomolecules to silver ions, indicating their active

TABLE 1: Larvicidal activity of *P.missionis*-derived AgNPs.

AgNPs concentration	PmL-AgNPs			PmB-AgNPs		
	No. of larvae died	Mortality rate (%)	IC_{50} and IC_{90}values	No. of larvae died	Mortality rate (%)	IC_{50} and IC_{90}values
10ppm	1.3 ± 0.6	6.7 ± 2.9		3.6 ± 1.5	18.3 ± 7.6	
20 ppm	4.3 ± 1.5	21.7 ± 7.6		5 ± 1	25 ± 5	
30 ppm	8 ± 1	40 ± 5		7 ± 1	35 ± 5	
50 ppm	11.6 ± 1.5	58.3 ± 7.6	42.88 (IC_{50})	10.3 ± 0.5	51.6 ± 2.8	48.45 (IC_{50})
80 ppm	14.3 ± 1.5	71.7 ± 7.6		14.3 ± 0.6	71.7 ± 2.9	
100ppm	**18.3 ± 0.6**	**91.7 ± 2.9**	**98.14 (IC_{90})**	**19 ± 1**	**95 ± 5**	**94.73 (IC_{90})**

PmL-AgNPs refers to leaf-mediated silver nanoparticles, PmB-AgNPs refers to bark-derived silver nanoparticles (Values= Mean ± Standard deviation).

TABLE 2: Photocatalytic dye degradation by AgNPs from *P. missionis.*

Time interval	PmL-AgNPs			PmB-AgNPs		
	O.D	Percentage	IC_{50} and IC_{90}values	O.D	Percentage	IC_{50} and IC_{90}values
5 min	0.465 ± 0.002	64.61 ± 0.19	7.73 mg (IC_{50})	0.520 ± 0.001	60.45 ± 0.07	8.27 mg (IC_{50})
15 min	0.324 ± 0.003	75.33 ± 0.23		0.502 ± 0.002	61.79 ± 0.16	
30 min	0.29 ± 0.002	77.94 ± 0.20		0.447 ± 0.002	65.95 ± 0.12	
60 min	0.237 ± 0.003	81.97 ± 0.2		0.387 ± 0.002	70.59 ± 0.16	
90 min	0.218 ± 0.002	83.4 ± 0.16		0.349 ± 0.001	73.43 ± 0.11	
120 min	0.193 ± 0.002	85.3 ± 0.15	10.55 mg (IC_{50})	0.282 ± 0.001	78.53 ± 0.11	11.46 mg (IC_{50})

PmL-AgNPs refers to leaf-derived silver nanoparticles, PmB-AgNPs refers to bark-derived silver nanoparticles (Values= Mean ± Standard deviation).

role in nanoparticle reduction and stabilization.

DLS showed size distributions of 2–100 nm (mode: 12.4 nm, PDI: 0.348) for PmL-AgNPs (Fig. 9) and 40–200 nm (mode: 77.4 nm, PDI: 0.337) for PmB-AgNPs (Fig. 11). The relatively low PDI values (~0.3) indicate uniformity and suitability for biomedical appli-cations. Notably, leaf-derived AgNPs exhibited much smaller particle sizes, which are advantageous for higher reactivity and biological uptake.

Zeta potential analysis revealed negative values of –15.9 mV for PmL-AgNPs (Fig. 10) and –17.6

mV for PmB-AgNPs (Fig. 12). These values indicate electrostatic repulsion between particles, preventing aggregation and ensuring colloidal stability. Bark-derived AgNPs showed slightly higher stability due to a more negative potential.

TEM analysis confirmed predominantly spherical morphology. Particle sizes ranged from 10–40 nm for PmL-AgNPs (Figs 13, 14) and 10–30 nm for PmB-AgNPs with clear lattice fringes on their surfaces (Figs 15, 16). The nanoscale dimensions and well-defined spherical shape support their potential for catalytic and biological applications.

Larvicidal activity was significant from 50 ppm onwards (Table 1). At this concentration, PmL-AgNPs caused 58.3% mortality, while PmB-AgNPs caused 51.6%, with corresponding IC_{50} values of 42.88 ppm and 48.45 ppm, respectively (Figs 17, 20). At 100 ppm, PmB-AgNPs achieved 95% mortality compared to 91.7% for PmL-AgNPs, with IC_{90} values of 94.45 ppm and 98.14 ppm, respectively (Figs 19, 22). These results indicate that bark-derived AgNPs were more effective at higher concentrations, highlighting their stronger larvicidal potential.

Photocatalytic activity against methylene blue dye showed rapid degradation within the first 5 min, with PmL-AgNPs achieving 64% and PmB-AgNPs 60% degradation, corresponding to IC_{50} values of 7.73 and 8.27, respectively (Fig. 23, Table 2). After 120 min, PmL-AgNPs reached 85% degradation, while PmB-AgNPs achieved 78%, with IC_{90} values of 10.55 and 11.46, respectively. These findings highlight the superior photocatalytic efficiency of leaf-derived AgNPs compared to bark-derived AgNPs.

DISCUSSION

The successful synthesis AgNPs using *P. missionis* leaf and bark extracts was evidenced by the colour change of the reaction mixture and further confirmed by UV-Vis, FTIR, DLS, zeta potential, and TEM analyses. The UV-Vis absorption peaks at 429–439 nm corresponds to SPR, a characteristic feature of AgNPs, consistent with earlier reports on plant-mediated AgNP synthesis (Huq et al. 2022, Yugandhar et al. 2015). Slight differences in SPR positions between leaf- and bark-derived AgNPs suggest that the phytochemical composition of the extracts influenced particle size and stability.

DLS analysis revealed that leaf-derived AgNPs were smaller (2–100 nm, mode 12.4 nm) and more uniform compared to bark-derived AgNPs (40–200 nm, mode 77.4 nm). Nanoparticles below 150 nm are generally preferred for enhanced cellular uptake and catalytic activity (Danaei et al. 2018), suggesting the greater applicability of leaf-derived AgNPs. TEM confirmed their predominantly spherical morphology, while zeta potential values (~ –16 to –18 mV) indicated sufficient electrostatic repulsion to prevent aggregation, consistent with stable colloidal dispersions. FTIR spectra demonstrated the involvement of functional groups such as alcohols, carboxylic acids, amines, and alkenes in nanoparticle reduction and stabilization. The shifts and disappearance of certain peaks in AgNPs

compared to crude extracts provide strong evidence for the binding of phytochemicals to silver ions during synthesis, a trend also reported in similar plant-based systems (Malik et al. 2023).

The larvicidal assays demonstrated dose-dependent mortality of mosquito larvae, with significant effects observed from 50 ppm onwards. At 100 ppm, bark-mediated AgNPs achieved 95% mortality compared to 91.7% for leaf-derived AgNPs, indicating slightly higher larvicidal potential of bark extracts at higher concentrations. Similar larvicidal effects of AgNPs synthesized from other medicinal plants have been documented (Mahalingam et al. 2023), supporting the use of green-synthesized AgNPs as eco-friendly mosquito control agents. The higher efficacy of bark-derived AgNPs may be attributed to phytochemicals like propiolic acid, arsenous acid, tris (trimethylsillyl) ester etc. that enhance interactions with larval membranes, leading to mortality (Yaswanthi et al. 2024).

In contrast, photocatalytic studies revealed superior performance of leaf-derived AgNPs, which achieved 85% degradation of methylene blue within 120 min, compared to 78% for bark-derived AgNPs. The smaller size of leaf-derived nanoparticles provides a higher surface-to-volume ratio, facilitating faster electron transfer and improved photocatalytic efficiency under sunlight. Similar trends of enhanced photocatalytic activity with plant-mediated AgNPs have been reported in earlier studies (Yugandhar et al. 2019, Rama et al. 2023).

Our previous work with *P. missionis* plant powders demonstrated photocatalytic efficiencies of 80.5% for leaves and 72.88% for bark (Yaswanthi et al. 2024). The present results with AgNPs not only confirm this trend but also show a clear enhancement in dye degradation efficiency. This improvement may be attributed to the nanoscale dimensions of AgNPs, which increase surface reactivity, along with the contribution of leaf phytochemicals such as phenols, flavonoids, and tannins. Furthermore, essential micronutrients including zinc, copper, and iron, previously identified in the plant powders, synergize with AgNPs to further boost photocatalytic activity.

Overall, these results highlight that *P. missionis*-derived AgNPs offer a dual advantage: bark-derived AgNPs provide stronger larvicidal activity at 100 ppm concentration, while leaf-derived AgNPs demonstrate superior photocatalytic efficiency at 10 mg concentration after 120 min. The study underscores the potential of *P. missionis* as a novel bioresource for sustainable nanotechnology, bridging environmental remediation and public health applications.

ACKNOWLEDGMENT

We thank Dr. V. Subbaiah, DST PURSE Centre, Sri Venkateswara University, Tirupati for his help in the characterization of synthesized nanoparticles.

Declaration

Authors' contribution

Plant collection, synthesis, experimen-tation, and data analysis were carried out by MSY. Manuscript writing was

assisted by RBA and SA; drafting and revision of the manuscript were done by NS.

Conflict of interest

Authors declare no conflict of interest.

REFERENCES

ABBAS R, LUO J, QI X, NAZ A, KHAN I A, LIU H, YU S & WEI J 2024 Silver nanoparticles: synthesis structure properties and applications *Nanomaterials* **14** 1425 https://doi.org/10.3390/nano14171425

BENELLI G, JEFFRIES C L & WALKER T 2016 Biological control of mosquito vectors: Past present and future *Insects* **7** 52 https://doi.org/10.3390/insects7040052

BHARATHI J D & SUSEEM S R 2024 Larvicidal activity of CuO and ZnO nanoparticles against *Aedes aegypti* and *Anopheles stephensi* mosquito vectors-a greener approach by *Phaseolus vulgaris* L aqueous extract as bio-reductant *Results Chemistry* **7** 101408

DANAEI M, DEHGHANKHOLD M, ATAEI S, HASANZADEH DAVARANI F, JAVANMARD R, DOKHANI A, KHORASANI S & MOZAFARI M R 2018 Impact of particle size and polydispersity index on the clinical applications of lipidic nanocarrier systems *Pharmaceutics* **10** 57 doi: 10.3390/pharmaceutics10020057

HUQ M A, ASHRAFUDOULLA M, RAHMAN M M, BALUSAMY S R & AKTER S 2022 Green synthesis and potential antibacterial applications of bioactive silver nanoparticles: A Review *Polymers* **14** 742 https://doi.org/10.3390/polym14040742

JAYAWEERA D M A 1982 *Medicinal plants (indigenous and exotic) used in Ceylon* National Science Council of Sri Lanka Columbo

MAHALINGAM S, GOVINDARAJI P K, SOLOMON V G, KESAVAN H, NEELAN Y D, BAKTHAVATCHALAM S, KIM J & BAKTHAVATCHALAM P 2023 Biogenic synthesis and characterization of silver nanoparticles: Evaluation of their larvicidal antibacterial and cytotoxic activities *ACS Omega* **8** 11923–11930

MALIK S, MUHAMMAD K & WAHEED Y 2023 Nanotechnology: A revolution in modern Industry *Molecules* **28** 661 doi.org/10.3390/molecules28020661

NAIK B R, TYAGI B K & RUI DE XUE 2023 Mosquito-borne diseases in India over the past 50 years and their global public health implications: A systematic review *J Am Mosq Contr Assoc* **39** 258–277

OKOYE U C, ARHEWOH M I & OKHAMAFE A O 2022 Synthesis characterization and applications of nanoparticles *Int J Pharmaceut Sci Rev Res* **77** 14–20

ONEN H, LUZALA M M, KIGOZI S, SIKUMBILI R M, MUANGA C K, ZOLA E N, WENDJI S N, BUYA A B, BALCIUNAITIENE A, VIŠKELIS J, KADDU-MUKASA M A & MEMVANGA P B 2023 Mosquito-borne diseases and their control strategies: An overview focused on green synthesized plant-based metallic nanoparticles *Insects* **14** 221 DOI: 10.3390/insects 14030221

PIYAWAN N, ARNANNIT K, PAWEENA P, RUNGNAPA P, SAKSIT C & PRAWIT N 2023 Efficient degradation of dye pollutants in wastewater via photocatalysis using a magnetic zinc oxide/graphene/iron oxide-based catalyst *Water Sci Eng* **16** 243–251

RAMA P, MARISELVI P, SUNDARAM R & MUTHU K 2023. Eco-friendly green synthesis of silver nanoparticles from *Aegle marmelos* leaf extract and their antimicrobial antioxidant anticancer and photocatalytic degradation activity *Heliyon* **9** 16277

RANIA A, SAMEH S A, FANGHUA L, KAMAL M O, YEHIA A G M, TAMER E, HAIXIN J, YINYI F & JIANZHONG S 2022 A critical review on the treatment of dye-containing wastewater: Ecotoxicological and health concerns of textile dyes and possible remediation approaches for environmental safety *Ecotoxicol Env Safety* **231** 113160

SADIA K, TAYYABA N, NASEEM I & LUBNA Y 2024 Photocatalytic dye degradation from textile waste water: A Review *ACS Omega* **9** 21751–21767

SAXENA S K, ELAHI A, GADUGU S & PRASAD A K 2016 Zika virus outbreak: an overview of the experimental therapeutics and treatment *Virus Disease,* **27** 111–115

SOMASUNDARAM T R 1967 *A Handbook on the identification and description of trees shrubs and some important herbs of the forests of the southern states: For the use of the southern forest rangers college* Southern Forest Rangers College Coimbatore

VENKATESWARLU P, ANKANNA S, PRASAD T N V K V, ELUMALAI E K, NAGAJYOTHI P C & SAVITHRAMMA N 2010 Green synthesis of silver nanoparticles using *Shorea tumbuggaia* stem bark *Int J Drug Dev Res* **2** 720–723

YASWANTHI M S, PALLAVI P & SAVITHRAMMA N 2024. Qualitative and quantitative metabolomics of *Pamburus missionis* Swingle – a medicinal tree taxon *J Med Herbs Ethnomedi* 7–11

YUGANDHAR P, HARIBABU R & SAVITHRAMMA N 2015 Synthesis characterization and antimicrobial properties of green-synthesized silver nanoparticles from stem bark extract of *Syzygium alternifolium* (Wt) Walp *3 Biotech* **5** 1031–1039

YUGANDHAR P, VASAVI T, BHASHA S, UMA MAHESWARI DEVI P, SATHYAVELU REDDY K & SAVITHRAMMA N 2019 Biofabrication characterization and evaluation of photocatalytic dye degradation efficiency of *Syzygium alternifolium* leaf extract mediated copper oxide nanoparticles *Mater. Res. Express* **6** 065034

ZARGHAM F, AFZAL M, RASOOL K, MANZOOR S & QURESHI N A 2023. Larvicidal activity of green synthesized iron oxide nanoparticles using *Grevillea robusta* Cunn leaf extract against vector mosquitoes and their characterization *Exp Parasitol* **252** 108586

Journal of Cytology and Genetics 2025 VOL. **26** (NS): 49−59

RESEARCH ARTICLE

HIERARCHICAL CLUSTER ANALYSIS OF *CARDIOSPERMUM HALICACABUM* L.: INSIGHTS INTO GENETIC DIVERSITY[$]

V. VIJITHA[1], CINTHYA CHRISTOPHER[2]*, D. G. SMITHA[3]

[1]Post-graduate and Research Department of Botany, Christian College, Kattakada, University of Kerala,Thiruvananthapuram 695 572, India

[2]Department of Botany, All Saints' College,University of Kerala, Thiruvananthapuram 695 007, India

[3]Department of Botany, University College, University of Kerala, Thiruvananthapuram 695 034, India

*For correspondence. Email: cinthya_wilfred@yahoo.com

(Received 10 October 2025, accepted 25 October 2025)

SUMMARY Extensive morphological variation was observed among *Cardiospermum halicacabum* accessions collected from Kerala. To evaluate this diversity, frequency distributions of character states were analyzed and the accessions were subjected to Ward's minimum variance clustering analysis based on these characters, incorporating both qualitative and quantitative traits. The resulting dendrogram classified the accessions into 10 distinct clusters at a 55.8% similarity threshold, with cluster sizes ranging from 1 to 13 members. The clustering analysis revealed considerable intracluster similarity (connectedness) and intercluster divergence (isolation), indicating well-defined groupings. This morphological differentiation pattern has significant genetic implications, providing a strategic framework for selecting parental genotypes with substantial genetic divergence. Selections from isolated clusters can be effectively utilized in intraspecific hybridization programmes to exploit heterosis and enhance crop improvement in *C. halicacabum.*

Keywords: *Cardiospermum halicacabum*, frequency distribution, hierarchial cluster analysis, genetic implication, similarity matrix, Euclidean distance percentage.

INTRODUCTION

Cardiospermum halicacabum, commonly known as balloon vine, is a dioecious member of the family Sapindaceae. This species is distinguished by its trifoliate leaves, slender hairy stems, and inflated capsule like fruits. *C. halicacabum* used traditionally in different systems of medicine such as Ayurveda, Homeopathy and Unani. (Mohaddesi & Dudhrejiya 2016). This herb acts as a diaphoretic, diuretic, emetic, laxative, refrigerant, stomachic and sudorific and has antibacterial, antidiarrheal, antioxidant activities, suppress Tumor Necrosis Factor production (Babu & Krishnakumari 2006), exhibits anticancer and vaso depressant effect. This

[$]Paper presented at the XV All India Conference on Cytology and Genetics held on 11th and 12th September 2025.

herb is also useful in curing of rheumatism, severe bronchitis and snakebite (Rao et al. 2006). Antiulcer, analgesic, antiparasitic, antimalarial, antifilarial, and antipyretic role were also accounted for this herb (Muthumani et al. 2010). *C. halicacabum* is also an ingredient of many plant-based products released by various companies across the world like in "Allergy Relief Liquid™", "Bioforce Pollinosan® Tabs" marketed by Bioforce, USA and "Florasone Cardiospermum Cream" released by US based company Boericke and Tafel. (Subrahmanyam et al. 2007).

The National Medicinal Plants Board has been supporting the conservation and cultivation of *C. halicacabum.* It is among the 59 self-grown species in high trade sourced from natural habitats. The population of *C. halicacabum* is declining due to overcollection to meet rising commercial and household demand (Goraya & Ved 2017).

Numerous studies in intraspecific taxonomy have primarily relied on conspicuous traits of gross morphology. While variation in these characters has informed both formal and informal diagnostic classifications, such approaches may overlook subtler traits that hold significant taxonomic value. Effective examples of intraspecific classifications in crop plants include the work of Rogers & Fleming (1973) on South American cultivars of cassava (*Manihot esculenta*), Martin & Rhodes (1977) on yams (*Dioscorea alata*), Mathew et al. (2001) on black pepper (*Piper nigrum*), Subramanian & Subbaraman (2010) on maize germplasm, Tomsone et al. (2012) on horseradish genotypes (*Armoracia rusticana*), and Christopher et al. (2019) on Brahmi (*Bacopa monnieri*). Intermediate clusters are often inevitable in intraspecific analyses, and a robust clustering technique should be capable of identifying and delineating all such groupings. Several methods have been employed to establish taxonomically sound intraspecific clusters, among which hierar-chical clustering particularly, Ward's minimum variance method which is widely recognized as a reliable approach. It is especially effective in identifying promising accessions or cultivars for selection and in choosing putative parents for intervarietal crossing.

Widespread across tropical regions, *C. halicacabum* exhibits considerable genetic diversity, making it a valuable resource for morphological characterization and accession level selection. Various methods have been developed for establishing taxonomically sound intraspecific clusters, of which the hierarchical clustering method — Ward's minimum variance cluster analysis — is recognized as a fairly viable and helpful approach for identifying prospective accessions/cultivars in screening for selection and choosing putative parents for intervarietal crossing. This method has been applied in the present study for clustering 68 accessions of *C. halicacabum*, collected from across the state of Kerala, to sort them into clusters with fair degrees of intracluster similarity and intercluster isolation. In addition to creating a viable grouping of the accessions, the results are also useful for selecting accessions with an appreciable degree of

genetic divergence for future genetic improvement programme through hybridization in the species.

MATERIALS AND METHODS

Field surveys were conducted to locate and collect accessions of *C. halicacabum* from diverse eco-geographical regions of Kerala (Table 1). Habitat observations, associated flora, and other relevant characteristics were documented in standardized passport data sheets. Planting materials collected during the field surveys were established in the Field Gene Bank of Christian College Kattakada, Thiruvananthapuram. Conservation and maintenance of the accessions followed standardized agronomic practices.

The 68 accessions were established in a field gene bank under uniform environmental conditions to ensure consistent growth and minimize environmental variation affecting trait expression. Morphological characterization data were collected for 35 characters, comprising 15 qualitative traits (Table 2) and 20 quantitative traits (Table 3). The data were pooled, standardized, and subjected to statistical analysis. Ward's minimum variance cluster analysis (Szekely & Rizzo 2005) was conducted using SAS software. Variability in qualitative traits was assessed based on the number of character states expressed by each accession. A similarity matrix was generated using Euclidean distance measures between accession pairs through the PROC procedure, which was subsequently used to construct a dendrogram illustrating the genetic relationships among the accessions.

OBSERVATIONS

The hierarchical clustering of 68 *C. halicacabum* accessions is illustrated in the dendrogram (Fig. 1). Based on an arbitrarily selected phenetic threshold of 55.8% similarity, 10 distinct clusters were delineated (Table 4). These clusters represent maximally connected subgroups, each comprising accessions with relatively high morphological similarity. The number of accessions per cluster varied, ranging from 1 in Cluster III to 13 in Cluster I and X. The similarity matrix reveals varying degrees of genetic resemblance among the 68 accessions of *C. halicacabum*, indicating both closely related and genetically diverse groups. Correspondingly, the Euclidean distance percentages further illustrate this diversity, with accessions clustering into distinct groups based on their genetic distances, suggesting potential subpopulations or ecotypes within the species.

TABLE 2: Character states of the 15 qualitative characters observed in the 68 accessions of *C. halicacabum.*

Sl. No.	Character	Character states
1	Stem colour	Green, Reddish-brown
2	Leaf colour	Green, Pale-green
3	Leaf shape	Ovate lanceolate, lanceolate
4	Leaf apex	Acute, acuminate
5	Leaf margin	Lobed, serrate
6	Leaf texture	Delicate, pubescent
7	Leaf arrangement	Pinnately, palmately
8	Flower colour	White, yellowish
9	Sepal colour	Green, reddish
10	Petal shape	White, greenish
11	Stigma colour	Yellow, pale yellow
12	Stamen colour	Creamy white, yellowish
13	Ovary colour	Light green, yellowish-green
14	Fruit capsule colour	Light green, pale pink
15	Seed colour	Black with white heart shape, Grey with white heart shape

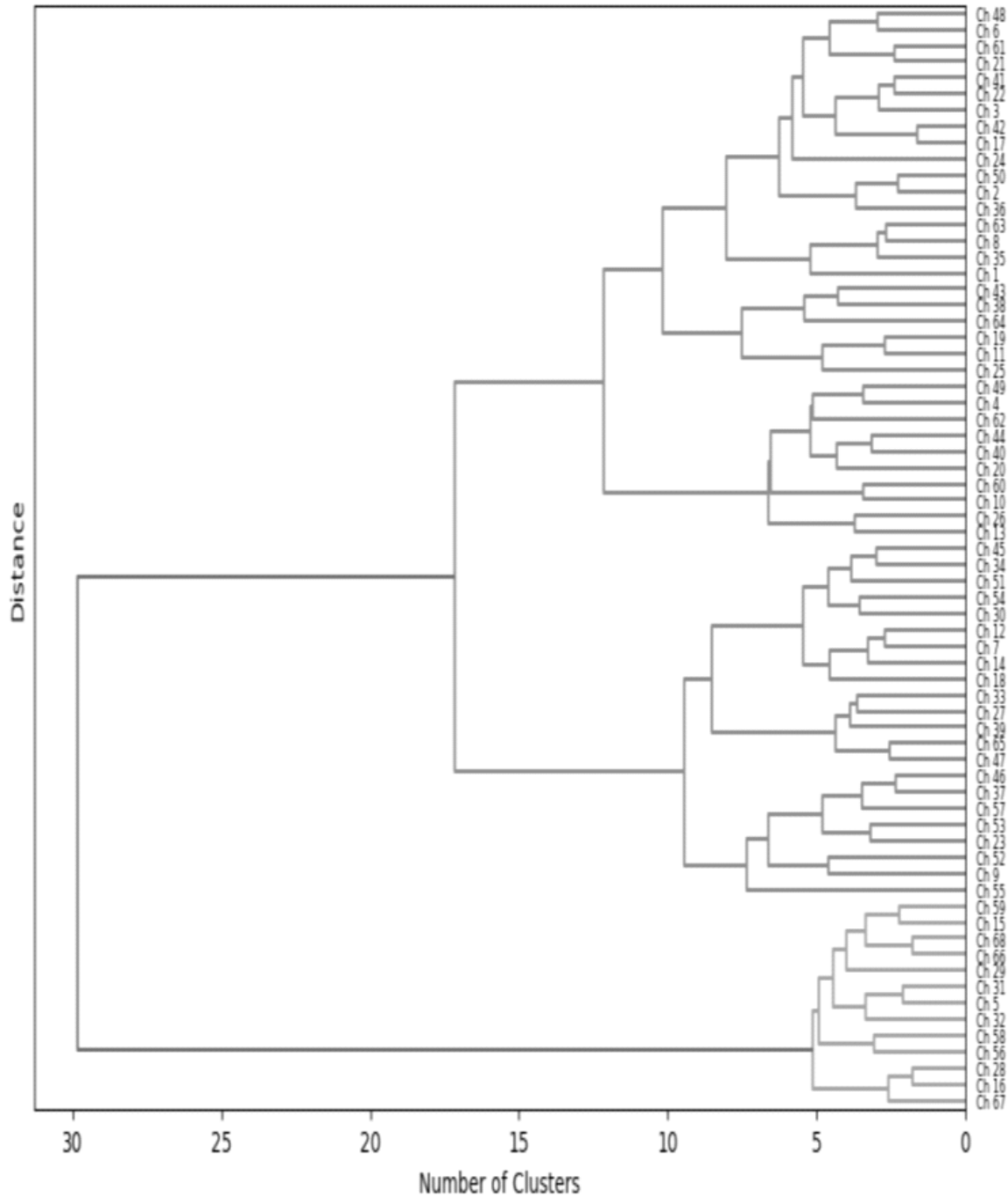

Fig. 1: Dendrogram showing ten clusters of *C. halicacabum* formed by hierarchical cluster analysis.

TABLE 1: Details of localities of the 68 accessions of *C. halicacabum.*

Acc. No.	Place of collection	District	Acc. No.	Place of collection	District
Ch 1	Kovalam	Trivandrum	Ch 24	Kanjirappally	Kottayam
Ch 2	Palayam	Trivandrum	Ch 25	Kumarakom	Kottayam
Ch 3	Nedumangad	Trivandrum	Ch 26	Muvattupuzha	Ernakulam
Ch 4	Thirumala	Trivandrum	Ch 27	Aluva	Ernakulam
Ch 5	Ponmudi	Trivandrum	Ch 28	Thevara	Ernakulam
Ch 6	Kuttikkadu	Kollam	Ch 29	Malayattoor	Ernakulam
Ch 7	Kottarakkara	Kollam	Ch 30	Peermade	Idukki
Ch 8	Punalur	Kollam	Ch 31	Adimali	Idukki
Ch 9	Munroe Island	Kollam	Ch 32	Idukki Twp	Idukki
Ch 10	Thangassery	Kollam	Ch 33	Anavilasam	Idukki
Ch 11	Adoor	Pathanamttitta	Ch 34	Vandiperiyar	Idukki
Ch 12	Konni	Pathanamttitta	Ch 35	Pananchery	Thrissur
Ch 13	Mallappally	Pathanamttitta	Ch 36	Edakkara	Thrissur
Ch 14	Ranni	Pathanamttitta	Ch 37	Kottappuram	Thrissur
Ch 15	Chittar	Pathanamttitta	Ch 38	Kolazhy	Thrissur
Ch 16	Chunakkara	Alappuzha	Ch 39	Pullur	Thrissur
Ch 17	Karuvatta	Alappuzha	Ch 40	Panangattiri	Palakkad
Ch 18	Ambalapuzha	Alappuzha	Ch 41	Pathirippala	Palakkad
Ch 19	Mararikulam	Alappuzha	Ch 42	Kinassery	Palakkad
Ch 20	Cherthala	Alappuzha	Ch 43	Mannarkad-i	Palakkad
Ch 21	Ettumanoor	Kottayam	Ch 44	Kulakkad	Palakkad
Ch 22	Kondoor	Kottayam	Ch 45	Kodumudi	Malappuram
Ch 23	Vadavathoor	Kottayam	Ch 46	Varangode	Malappuram

(Continued)

TABLE 1: (Concluded).

Acc. No.	Place of collection	District	Acc. No.	Place of collection	District
Ch 47	Pandalur	Malappuram	Ch 58	Irulam	Wayanad
Ch 48	Mampad	Malappuram	Ch 59	Pulpally	Wayanad
Ch 49	Areekode	Malappuram	Ch 60	Thavinhal	Wayanad
Ch 50	Triprangode	Malappuram	Ch 61	Valiyannur	Kannur
Ch 51	Thamarassery	Kozhikode	Ch 62	Nuchiyad	Kannur
Ch 52	Kuttiady	Kozhikode	Ch 63	Taliparamba	Kannur
Ch 53	Iringal	Kozhikode	Ch 64	Pazhayangadi	Kannur
Ch 54	Chemancheri	Kozhikode	Ch 65	Muzhappilangad	Kannur
Ch 55	Azhinjilam	Kozhikode	Ch 66	Kallar	Kasargod
Ch 56	Madathumpadi	Wayanad	Ch 67	Kakkat	Kasargod
Ch 57	Kidanganad	Wayanad	Ch 68	Udma	Kasargod

TABLE 3: Measures of central tendency (Mean) and dispersion (Range) of the 20 quantitative characters of the 68 accessions of *C. halicacabum*.

Sl. No.	Character	Grand mean	Standard error	Range	Critical difference 1%	Critical difference 5%
1	Stem width (cm)	0.27 cm	0.01	0.20–0.37	0.0115	0.0119
2	Stem diameter (mm)	2.98 mm	0.05	2–4	0.1482	0.1116
3	Internodal length (cm)	7.12 cm	0.08	6.13–8.43	0.1651	0.1716
4	Tendril length (cm)	6.61 cm	0.05	6.10–7.53	0.0929	0.0965
5	Petiole length (cm)	1.73 cm	0.03	1.41–2.32	0.0505	0.0525
6	Leaf length (cm)	7.38 cm	0.09	5.90–8.57	0.1813	0.1884
7	Leaf breadth (cm)	5.35 cm	0.08	3.73–6.27	0.1653	0.1719
8	Leaf area (cm^2)	27.76 cm^2	0.61	13.5–36.19	1.6290	1.2248
9	Number of dentations/leaves	45.02	0.21	41–47	0.4115	0.4278
10	Number of leaflets	8.90	0.02	8–9	0.0416	0.0433

(Continued)

TABLE 3: (Concluded).

Sl. No.	Character	Grand mean	Standard error	Range	Critical difference 1%	Critical difference 5%
11	Number of flowers	4.57 (Nos.)	0.12	3–6	0.228	0.2371
12	Flower length (mm)	4.02 cm	0.06	3.00–5.00	0.1196	0.1244
13	Petal length (mm)	2.26 cm	0.03	2.00–2.67	0.0689	0.0716
14	Number of petals	3.91 (Nos.)	0.02	3–4	0.0356	0.037
15	Sepal length (mm)	1.13 cm	0.02	1.00–1.67	0.0415	0.0432
16	Number of stamens	7.95 (Nos.)	0.01	7–8	0.0297	0.0309
17	Stamen filament length (mm)	1.56 cm	0.01	1.40–1.83	0.0294	0.0306
18	Fruit length (cm)	1.47 cm	0.03	1.13–1.93	0.066	0.0686
19	Fruit breadth (cm)	1.59 cm	0.03	1.23–2.00	0.0613	0.0637
20	Seed length (mm)	4.04 cm	0.07	3.00–5.00	0.1311	0.1363

DISCUSSION

The present study documented substantial morphological diversity among the 68 accessions of *C. halicacabum* collected from diverse ecogeographical regions across Kerala. The wide altitudinal range of collection sites (18–1104 m above sea level) contributed to the observed phenotypic variation, reflecting the species' remarkable adaptability to varied environmental conditions. The comprehensive sampling strategy encompassing all 14 districts of Kerala ensured representation of the species' morphological spectrum across different agroclimatic zones.

Analysis of the 15 qualitative characters revealed significant morphological polymorphism within the species. Notably, leaf type exhibited the highest uniformity, with 86.76% of accessions displaying pinnately compound leaves, suggesting this as a stable taxonomic character. In contrast, stamen colour showed maximum variation, with 88.24% of accessions possessing yellowish stamens compared to only 11.76% with creamy white stamens. This high degree of variability in reproductive structures may reflect adaptive responses to local pollinator preferences or environmental selective pressures.

Leaf morphological characters displayed considerable diversity, with 76.47% of accessions exhibiting lanceolate leaf shape and 66.18% showing pale green colouration. The predominance of acute leaf apex (69.12%) and serrate leaf margins (61.76%) suggest that these may represent adaptive traits for efficient light capture and reduced water loss in the tropical climate of Kerala. The delicate leaf texture observed in 75% of accessions likely contributes to drought tolerance, a crucial

adaptation for a climbing herb in variable moisture conditions.

The quantitative character analysis revealed normal to skewed distributions across the 20 measured traits. Stem width showed the highest coefficient of variation (CV = 25.93%), indicating substantial diversity in this vegetative character. Conversely, the number of stamens exhibited minimal variation (CV = 1.88%), reinforcing its taxonomic stability. The wide ranges observed in key morphometric characters, such as leaf length (5.90–8.57 cm) and fruit dimensions (1.13–2.00cm), underscore the plastic nature of *C. halicacabum* morphology.

Reproductive characters displayed moderate to high variability, with the number of flowers per inflorescence ranging from 3.00 to 6.67. This variation in reproductive output may reflect differences in resource allocation strategies among populations from contrasting environmental conditions. The consistency in petal number (3.67–4.00) across accessions confirms this as a conserved floral characteristic typical of the Sapindaceae.

The hierarchical cluster analysis at 55.8% similarity threshold resolved the 68 accessions into 10 distinct morphological groups, indicating considerable phenotypic diversity within the species. The largest cluster (Cluster I and X) contained 13 accessions primarily from the central and northern districts, suggesting possible common ancestry or similar selective pressures in these regions. Conversely, the singleton cluster (Cluster III) represented by accession Ch 55 from Kozhikode indicates unique morphological characteristics that may warrant further investigation for potential breeding value. This finding aligns with established patterns in plant genetic diversity studies, where traditional hierarchical clustering remains very popular in genetic diversity studies in plants due to its effectiveness in revealing population structure. The clusters obtained are well-defined, with their members possessing considerable discontinuity, meaning such clusters cannot be further subdivided. It is suggested that clusters with this property may be considered as maximal connected subgroups (Mathew et al. 2001). The distribution of various characters among the accessions showed a substantial degree of consistency within each cluster. The number of clusters obtained (10 clusters from 68 accessions) represents a moderate level of morphological differentiation, comparable to studies on other tropical plant species where cluster numbers typically range from 15–30% of total accessions analysed (Khadivi & Mirheidari 2024).

The cophenetic correlation coefficient and Ward's minimum variance method employed in this study follow best practices established in genetic diversity research. The cophenetic correlation coefficient is directly related to subgroup differentiation and can thus be used as an indicator of clustering quality.

The 55.8% similarity threshold selected appears appropriate, as it balances between overclustering (too many small groups) and underclustering (few large groups), consistent with

TABLE 4**:** Composition of clusters for the 68 accessions of *C. halicacabum* based on hierarchical cluster analysis.

Cluster	No. of accessions	Accession code
I	13	Ch 5, Ch 15, Ch 16, Ch 29, Ch 28, Ch 32, Ch 31, Ch 58, Ch 59, Ch 56, Ch 67, Ch 66, Ch 68
II	7	Ch 37, Ch 23, Ch 52, Ch 53, Ch 57, Ch 46, Ch 9
III	1	Ch 55
IV	5	Ch 33, Ch 47, Ch 27, Ch 65, Ch 39
V	9	Ch 18, Ch 30, Ch 54, Ch 34, Ch 45, Ch 51, Ch 12, Ch 7, Ch 14
VI	10	Ch 60, Ch 40, Ch 49, Ch 62, Ch 26, Ch 13, Ch 10, Ch 20, Ch 4, Ch 44
VII	3	Ch 25, Ch 11, Ch 19
VIII	3	Ch 43, Ch 64, Ch 38
IX	4	Ch 1, Ch 35, Ch 63, Ch 8
X	13	Ch 22, Ch 17, Ch 21, Ch 42, Ch 36, Ch 2, Ch 6, Ch 3, Ch 24, Ch 61, Ch 50, Ch 41, Ch 48

methodological guidelines for morphological trait-based clustering. The clustering pattern did not strictly follow geographical boundaries, with accessions from different districts often grouping together based on morphological similarity. This observation is consistent with findings in other crop genetic diversity studies where morphological clustering often transcends simple geographic boundaries. The presence of accessions from high altitude locations (Ponmudi – 1005 m, Anavilasam – 1104 m) in distinct clusters indicates altitudinal adaptation may influence morphological expression, supporting the concept of ecotypic differentiation in response to environmental gradients. The morphological diversity observed across Kerala's ecogeographical gradient reflects the species' evolutionary plasticity and local adaptation. The continuous variation in most quantitative traits suggests polygenic inheritance and environmental modulation of gene expression. The maintenance of high diversity within populations indicates effective gene flow and possibly outbreeding mating systems typical of climbing plants with animal mediated pollination.

The differential clustering of accessions from similar altitudes but different geographic locations suggests that local environmental pressures, soil types, and microclimatic conditions may be more

influential than broad geographic patterns in shaping morphological variation. This has important implications for conservation strategies, emphasizing the need to preserve populations across diverse habitats rather than focusing solely on geographic representation.

The documented morphological diversity represents a valuable genetic resource for potential crop improvement and conservation programs. The identification of distinct morphological clusters provides a framework for selecting representative accessions for core collection development. Accessions exhibiting extreme trait values, such as Ch 33 with the highest altitude adaptation (1104 m) or those with unique fruit characteristics, merit priority conservation status. The establishment of this field gene bank provides a foundation for systematic evaluation of agronomically important traits and potential medicinal properties. The morphological characterization data generated will facilitate efficient germplasm management and support future breeding programs aimed at developing improved varieties of this medicinally important species.

Comparative studies on crop genetic diversity using morphological traits have shown that the dissimilarity coefficient, as well as clustering method used for genetic diversity analysis, have implications on the result. The Ward's minimum variance method employed in this study is recognized as one of the most effective hierarchical clustering approaches for morphological data, as it minimizes within cluster variance while maximizing between cluster differences.

Despite the availability of newer approaches, traditional hierarchical clustering remains very popular in genetic diversity studies in plants, with the cophenetic correlation coefficient being directly related to subgroup differentiation. The effectiveness of this approach in the current study supports its continued relevance for morphological trait-based diversity assessment. The geographic distribution patterns observed in this study, where morphological similarity did not strictly correlate with geographic proximity, align with findings from other plant diversity studies. This suggests that adaptive responses to environmental factors may be more significant than isolation by distance in shaping morphological variation in *C. halicacabum.*

The study demonstrates that *C. halicacabum* populations in Kerala harbour substantial morphological diversity, likely representing significant genetic variation. This diversity should be considered in developing conservation strategies and exploitation programmes for this ethno-botanically important species. Further studies involving molecular markers would complement these morphological findings and provide insights into the genetic basis of observed phenotypic variation.

ACKNOWLEDGEMENT

The authors are grateful to the Principal and Management of Christian College, Kattakada for providing the facilities.

Declaration

The authors declare that this manuscript is original work and

has not been previously published or submitted elsewhere for publication.

Conflict of interest

All authors declare that no competing interests exist.

Consent to participate

All authors agree with the content of this manuscript and with all its publication.

REFERENCES

BABU V & KRISHNAKUMARI K C S 2006 *Cardiospermum halicacabum* suppresses the production of TNF-alpha and nitric oxide by human peripheral blood mononuclear cells *Afr J Biomed* **9** 95–99

CHRISTOPHER C, MATHEW P J, MATHEW P M & KUMAR V 2019 Hierarchial cluster analysis in *Bacopa monnieri* ans its genetic implications *J Cytol Genet* **20** (NS) 93–100

GORAYA G S & VED D K 2017 *Medicinal plants in India: An Assessment of their demand and supply* National Medicinal Plants Board and Ministry of AYUSH Government of India New Delhi

KHADIVI A, MIRHEIDARI F, TUNÇ Y, SAEIDIFAR A & MORADI Y 2025 Multivariate analysis of pomological and morphological diversity in *Withania coagulans* a neglected medicinal plant *Sci Rep* **15** 1–17

MARTIN F W & RHODES A M 1977 Intraspecific classification of *Dioscorea alata Trop Agri* **54** 1–13

MATHEW P J, MATHEW P M & KUMAR V 2001 Graph clustering of *Piper nigram* L *Euphytica* **118** 257–264

MOHADDESI B & DUDHREJIYA A 2016 Pharmacognostical and physico-chemical evaluations of *Cardiospermum halicacabum* L seeds *Res J Pharmacog* **3** 35–41

MUTHUMANI P, MEERA R, VENKATRAMAN S, GANAPATHY S & DEVI P 2010 Study of phytochemical analgesic and antiulcer activity of extracts of aerial parts of *Cardiospermum halicacabum* Linn IJPSR **10** 128–137

RAO V, CHANDRA P N K & SHANTA K S M 2006 Pharmacological investigation of *Cardiospermum halicacabum* (Linn) in different animal models of diarrhoea *Indian J Pharm* **38** 346–349

ROGERS D J & FLEMING H S 1973 A monograph of *Manihot esculenta* with an explanation of the taximetrics methods used *Econ Bot* **27** 1–113

SUBRAMANIAN A & SUBBARAMAN N 2010 Hierarchical cluster analysis of genetic diversity in maize germplasm *Electronic J Plant Breed* **1** 431–436

SUBRAMANYAM R, NEWMASTER S G, PALIYATH G & NEWMASTER C B 2007 Exploring ethnobiological classifications for novel alternative medicine: a case study of *Cardiospermum halicacabum* L (Modakathon Balloon Vine) as a traditional herb for treating rheumatoid arthritis *Ethnobotany* **19** 1–16

SZEKELY G J & RIZZO M L 2005 Hierarchical clustering via joint between within distances: Extending Ward's minimum variance method *J Classif* **22** 151–183

TOMSONE L, KRUMA Z, ALSINA I & LEPSE L 2012 The application of Hierarchical cluster analysis for classifying horseradish genotype (*Armoracia rusticana* L) roots *Chemine Technol* **4** 52–56

Journal of Cytology and Genetics 2025 VOL. **26** (NS): 61−72

RESEARCH ARTICLE

ENHANCING SEED GERMINATION AND SEEDLING GROWTH OF GREEN GRAM WITH BIOGENIC SILVER NANOPARTICLES FROM SEDGES**

G. BHAVANI*, S. ANKANNA AND N. SAVITHRAMMA

Department of Botany, Sri Venkateswara University, Tirupati 517 502, India

*For correspondence. Email: bhavanigetari76@gmail.com

(Received 27 September 2025, revised accepted 25 October 2025)

SUMMARY Advancements in nanotechnology have introduced innovative strategies in plant breeding, such as nano-priming and soil amendment, which enhance seed germination, promote uniform seedling emergence, and improve tolerance to abiotic stresses. This study has been focussed on application of biogenic silver nanoparticles (AgNPs), synthesized from various members of Cyperaceae, as an eco-friendly and sustainable approach to improving green gram (*Vigna radiata* L. (R.Wilczek) productivity. AgNPs were synthesized using aqueous extracts of *Kyllinga nemoralis* (J. R. Forst. & G. Forst.) Hutch & Dalz (KN) and *Fimbristylis ovata* (Burm.f.) J. Kern (FO) and characterized via UV-Vis spectroscopy, FTIR, dynamic light scattering (DLS), Zeta potential analysis, and transmission electron microscopy (TEM), revealing nanoparticle sizes ranging from 1 to 150 nm, suitable for biological and catalytic functions.

To assess their impact on plant development, green gram seeds were nano-primed with AgNPs at concentrations ranging from 10–50 ppm, and both in vitro germination and subsequent plant growth were evaluated over 35 d. Significant improvements in germination percentage, root length, and shoot length were observed up to 30 ppm, while concentrations above 30 ppm led to reduced growth and a lethal effect at 50 ppm. In vitro, KN-derived AgNPs at 10 ppm, FO-derived AgNPs at 20 ppm recorded the highest germination rate (98%), while KN-derived AgNPs yielded the longest root of 9.3 cm and shoot of 2.0 cm lengths. In soil amendment studies, KN-derived AgNPs resulted in the highest root length of 19.2 cm, while FO- derived AgNPs promoted the greatest shoot length of 35.3 cm.

Overall, biogenic AgNPs from cyperaceous taxa significantly enhanced early growth parameters in green gram, underscoring their potential as a nano-enabled tool in modern plant

** Paper presented at the XV All India Conference on Cytology and Genetics held on 11th and 12th September 2025

breeding. This integrative approach bridges traditional breeding with advanced nanotechnology to support climate-resilient and high-yielding agricultural systems.

Keywords: *Vigna radiata*, silver nanoparticles, seed germination, seedling growth, Cyperaceae.

INTRODUCTION

Germination is the first step in a plant life turning a dormant embryo into an active seedling and plays a vital role in subsequent growth as it initiates the life cycle of a new plant providing it with necessary hydration, nutrients and oxygen to emerge from seed and establish a healthy root and shoot systems. Effective and healthy seed germination is essential for producing high yields of crops, ensuring food stability and supporting agricultural economies and promotes genetic diversity in plant populations and long term health of ecosystems (Allesandra Francini & Antonio Ferrante 2023). However, the success of germination and seedling growth is not determined by biological factors alone; it is also shaped by the agricultural practices adopted to meet rising food demands. Among these, the use of chemical fertilizers has become a key intervention, with significant implications—both positive and negative for the germination process.

The explosion of population around the world since 20th century especially in India put a pressure on production of food grains and vegetables. This pressure, especially during and after the green revolution, led to the widespread adoption of synthetic fertilizers rich in nitrogen, phosphorus, and potassium, which could quickly replenish soil nutrients and support high-yielding crop varieties (Chittora et al. 2023). The soluble salts from fertilizers increase soil salinity, creating osmotic stress that draws water out of seeds, slowing or preventing imbibition, the first step of germination. This can cause seed desiccation or "fertilizer burn," reducing germination rates (Hajare & Akole 2022). The ongoing deterioration of soil fertility calls for an urgent need to identify innovative approaches that can improve seed germination and promote healthy robust seedling establishment.

Biogenic nanoparticles, synthesized using plants, microbes, or enzymes, offer a sustainable alternative to conventional fertilizers. Unlike bulk synthetic fertilizers, which often have a low nutrient-use efficiency, nanoparticles can be engineered for controlled nutrient release, and ensure plants to receive nutrients in the right form, time, and amount (Goyal et al.2023). Their nanoscale size enhances solubility and uptake, while their biological origin makes them more biodegradable and less harmful to soil microbes, reducing nitrate leaching and soil degradation (Arora et al. 2024). Replacing mineral nitrogen fertilizers with bio-nanoforms can cut nitrate accumulation in crops by up to 70% without yield loss (Abdelkader et al. 2024). Among them, silver nanoparticles (AgNPs) are notable for combining nutrient delivery with antimicrobial action, protecting seeds from pathogens and improving germination (Kale et al. 2021). They also help plants

tolerate stresses like drought or salinity (Alfosea-Simón et al. 2025), making them a multifunctional, ecofriendly option for integrated nutrient and pest management.

Phyto-sourced nanoparticles have been largely explored from dicots, yet many monocots especially Cyperaceae members remained underexplored. *Kyllinga nemoralis* employed in Ayurveda and folk medicine as a febrifuge, anti-diarrhoeal, stomachic, anti-helmintic (Abd Wahab & Abd Rahman 2022), and also used for treating rheumatism, hyperdipsia, fever, diarrhoea, worm infestations, cough, bronchitis, diabetes and fistula (SMPB databsase, Kerala). The other cyperaceaeous member, *Fimbristylis ovata* is used in Indian and African ethno-medicine for rheumatism, cough, bronchitis, asthma, urinary tract infections and arthritis. In Ayurveda, it is indicated for adenitis, scrofula, syphilis, and respiratory ailments (Pawade et al. 2018).

In the present study, AgNPs were green-synthesized using plant extracts of *K. nemoralis* and *F. ovata*. The resulting nanoparticles were thoroughly characterized and their effects evaluated on in vitro germination at concentrations ranging from 10 to 50 ppm, as well as on in vivo germination of *Vigna radiata* (green gram) over a 35d observation period.

MATERIALS AND METHODS

The plants of *K. nemoralis* and *F. ovata* were collected from Sri Venkateswara University Campus *GPS:* 13°62'89.276" N; 79°41'93.07" E. The whole plant material including roots and shoots are thoroughly washed, shade-dried for 20 d, powdered and stored for further studies.

Aqueous extracts were prepared by boiling 5 g of dried plant powder in 100 ml distilled water for 30 min, incubating for 24 h, and filtering through Whatman No. 1 paper. For the biosynthesis of silver AgNPs, 5 mL of the extract was combined with 50 ml of 1 mM silver nitrate ($AgNO_3$) solution and heated at 60° C to facilitate reduction. The reaction mixture was centrifuged at 10000 rpm for 20 min, and the resulting pellet was collected as purified AgNPs (Venkateswarlu et al. 2010, Yugandhar et al. 2015). The formation and physicochemical characteristics of the nanoparticles were analysed using ultraviolet–visible (UV-Vis) spectroscopy (200–800 nm), Fourier Transform Infrared Spectroscopy (FTIR), Dynamic Light Scattering (DLS), Zeta potential measurements and Transmission Electron Microscopy (TEM).

In vitro seed germination of green gram was examined by presoaking in water for 12 h and transferred to petri plates with serial concentrations of 10 ppm, 20 ppm, 30 ppm, 40 ppm and 50 ppm. Seed germination count, root length and shoot length were noted for 72 h. Based on the results from in-vitro seed germination; avoiding the lethal concentrations. The optimum concentrations for in vivo seedling growth was selected and over a period of 35 d root and shoot lengths are noted.

OBSERVATIONS

Upon the addition of aqueous plant extracts to the

$AgNO_3$ solution, a noticeable colour transition from yellowish-brown to dark brown was observed, indicating the successful formation of AgNPs (Figs 1, 2).

UV-Vis spectroscopy revealed strong surface plasmon resonance (SPR) peaks for KN-derived AgNPs at 427 nm and 433 nm for FO-derived AgNPs confirming nanoparticle formation. (Figs 3, 4).

FTIR data verification showed phytochemicals contributed to the reduction and stabilization of AgNPs (Figs 5–8). In KN extract peaks observed at

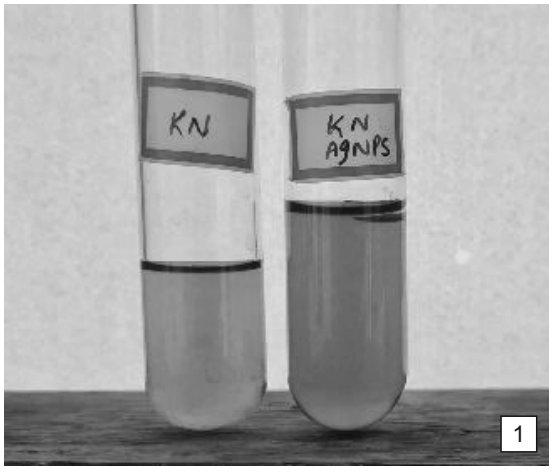

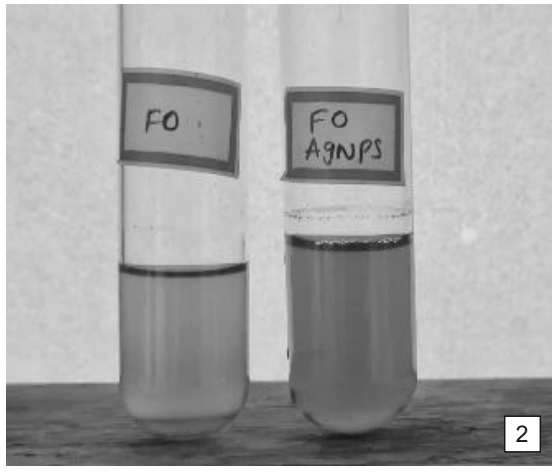

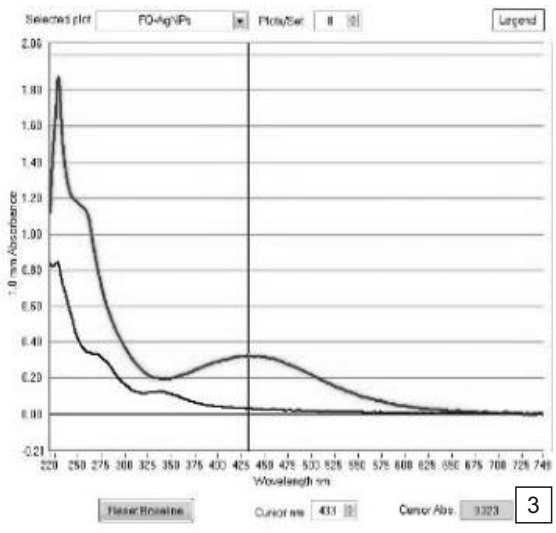

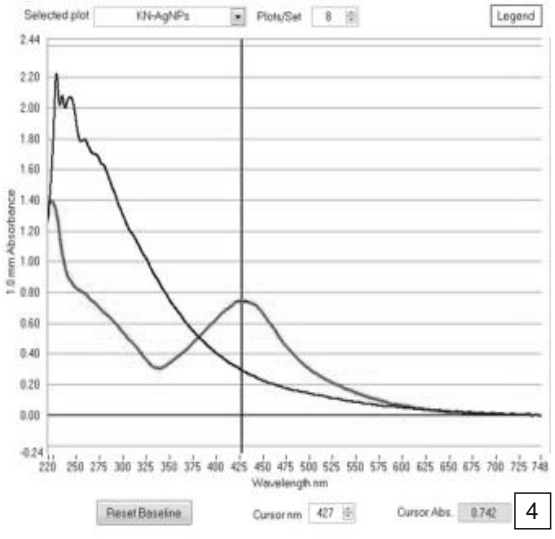

Figs 1–4: 1. AgNPs synthesis from *K. nemoralis* extract (KN-AgNPs). 2. AgNPs synthesis from *F. ovata* extract (FO-AgNPs). 3. UV-Vis peak of KN-AgNPs at 427 nm. 4. UV-Vis peak of FO-AgNPs at 433 nm.

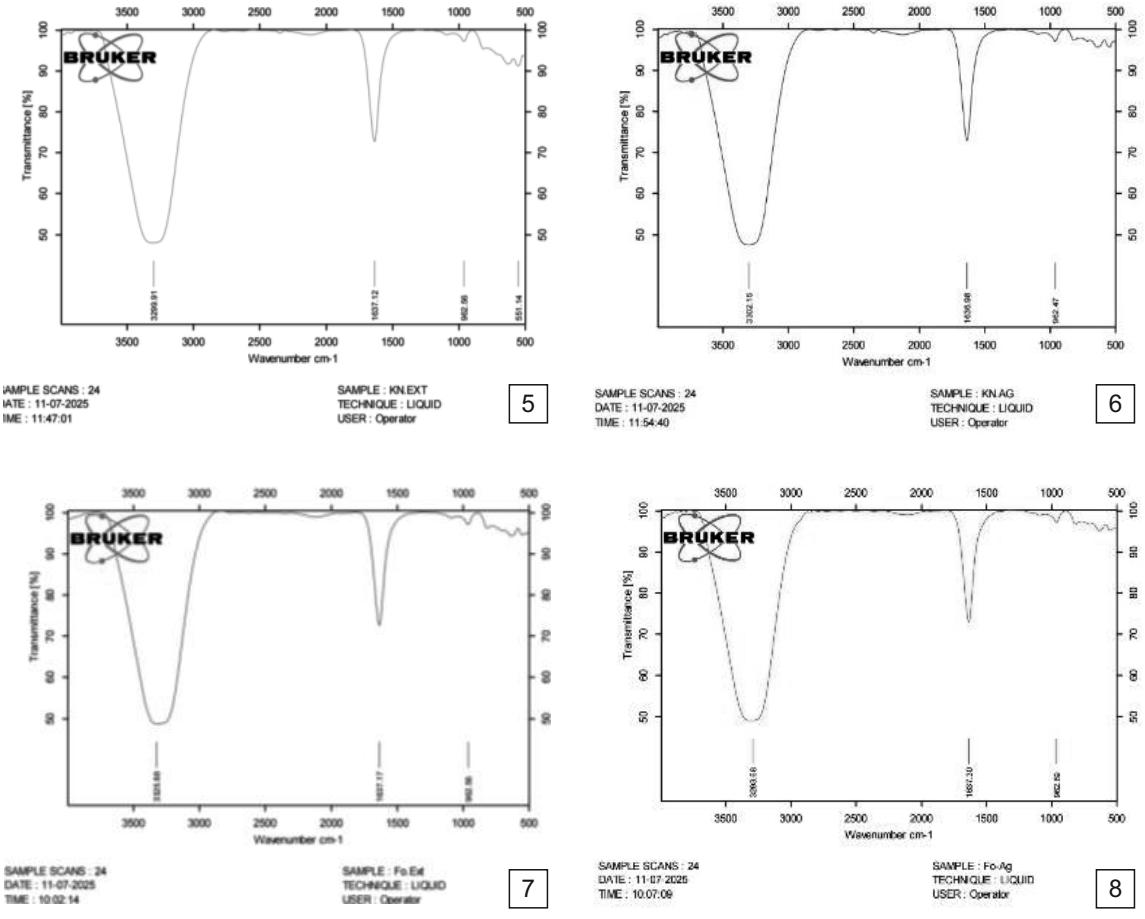

Figs 5–8: 5. FTIR peaks of KN extract. 6. FTIR peaks of KN-AgNPs. 7. FTIR peaks of FO extract. 8. FTIR peaks of FO-AgNPs.

3299 cm^{-1} (O-H stretching hydrogen bonded - alcohol), 1637 cm^{-1} (C = C alkene), 962 cm^{-1} (N – H amine), 551 cm^{-1} and the synthesized AgNPs peaks were observed at 3302 cm^{-1} (alcohol), 1637 cm^{-1} (alkene), 962 cm^{-1} (amine). For FO extracts, peaks were noted at 3326 cm^{-1} (alcohol), 1637 cm^{-1} (alkene), and 962 cm^{-1} (amine); for AgNPs, the peaks were noted at 3294 cm^{-1} (alcohol), 1637 cm^{-1} (alkene), and 963 cm^{-1} (amine).

Size distributions were characterized by DLS indicated the distribution of particle sizes for KN at 40 – 70 nm (mode: 49.9.4 nm, PDI: 1.430) and FO at 1 – 9 nm (mode: 1.2 nm, PDI: 0.261) (Fig. 4). Low PDI for FO suggests good colloidal stability whereas high PDI (>1.0) for KN may indicate rapid sedimentation which might still be useful in bulk coatings or catalysts following a careful validation. Lower particle size for FO regimes point to

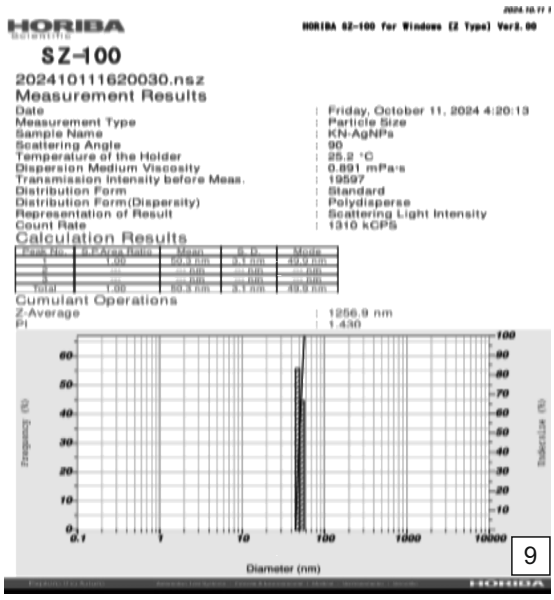

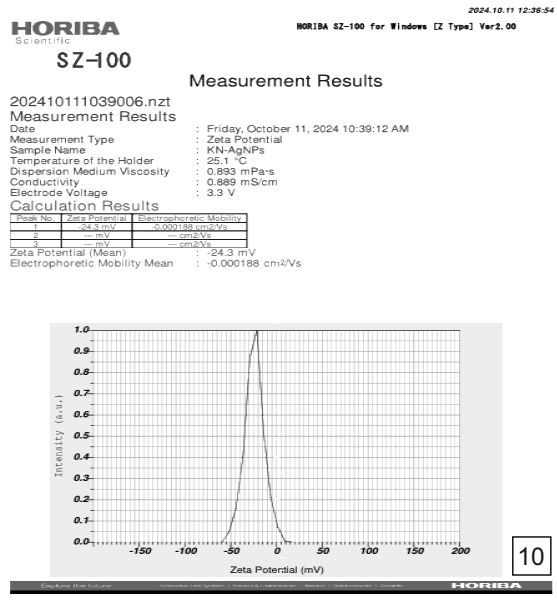

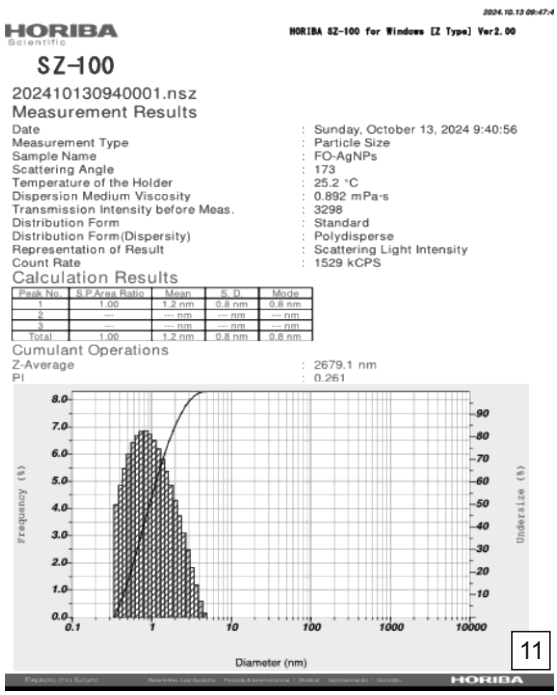

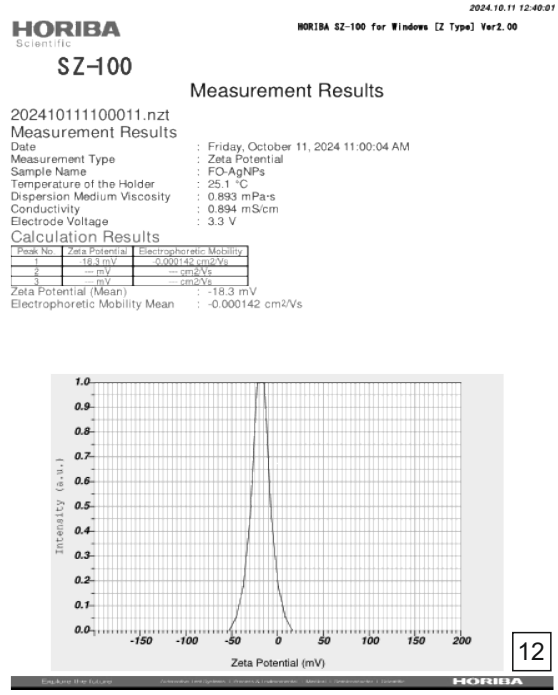

Figs 9–12: 9. The size range of KN-AgNPs from DLS (40–70 nm). 10. Surface charge of KN-AgNPs from Z-potential (–24.3 mV). 11. The size range of FO-AgNPs from DLS (1–9 nm). 12. Surface charge of FO-AgNPs from Z-potential (–18.3 mV).

specialized applications across biology, polymer science, catalysis, and sensing also in studies of protein–ligand interactions and enzyme kinetics at the single-molecule level, also in characterization of therapeutic oligonucleotides. The particles exhibited negative zeta potential values of -24.3mV for KN AGNPs indicating they are stable and particles may remain dispersed under gentle conditions but could aggregate under stress and -18.3mV for FO AGNPs indicating electrostatic repulsions and colloidal stability (Figs 9–12).

TEM micrographs demonstrated that the particles were primarily spherical, with a subset exhibiting different morphologies ranging from oval, spherical and irregular geometries. Defined lattices and clear demarcated images are noted at 50 nm and 20 nm magnifications (Figs 13–16). Particles size ranged from 12–60 nm for KN AgNPs whereas 7 to 60 nm for FO AgNPs with well-defined lattice fringes and side patterns.

In vitro assays conducted using petri plates over a 72 h observation period. This revealed a clear dose-dependent response marking the increased germination percentage and increased strength in roots and within the petri plates (Figs 17–20). This marked the enhanced growth in length and mechanical strength up to 30 ppm but significant reduction was observed after 30 ppm and lethality was observed at 50 ppm determining the concentration that causes mortality (Tables 1, 2). Based the results from experiments of in-vitro germination, optimum concentrations up to 30 ppm were selected for in-vivo studies by soil amendment and observed over a period of 35 d (Figs 21, 22). As a result, thick roots and strong shoots with high length were found at 20 ppm which was found to be optimum concentration for enhancing the seedling growth was noticed (Table 3).

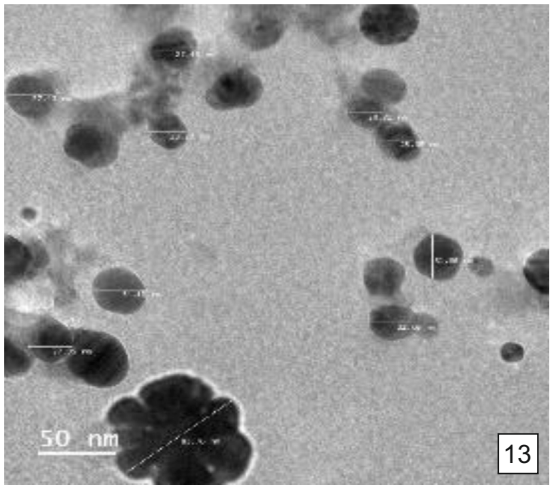

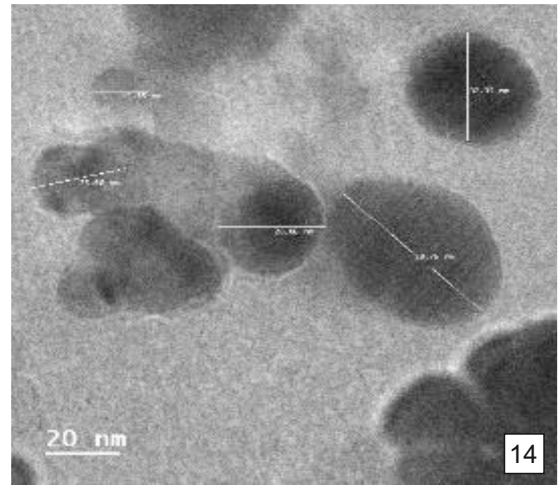

Figs 13 & 14: 13. TEM image of KN-AgNPs at 50nm magnification showing the sizes of AgNPs (12–60 nm). 14. TEM image of KN-AgNPs at 20nm magnification.

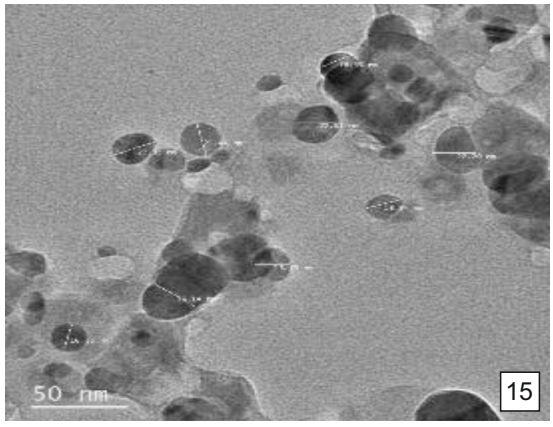

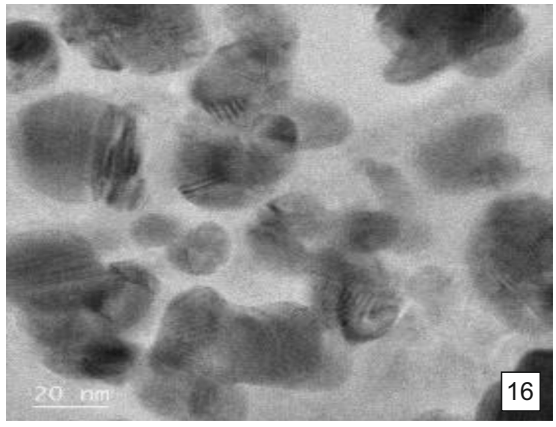

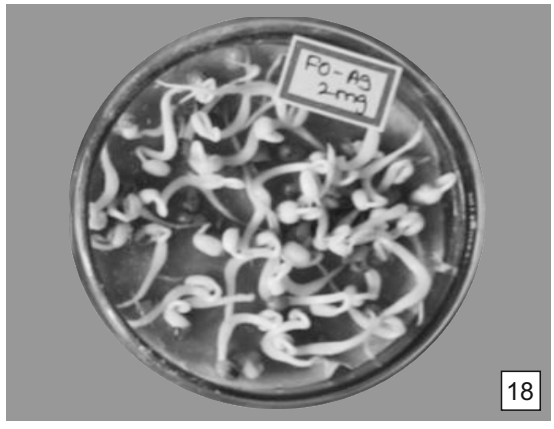

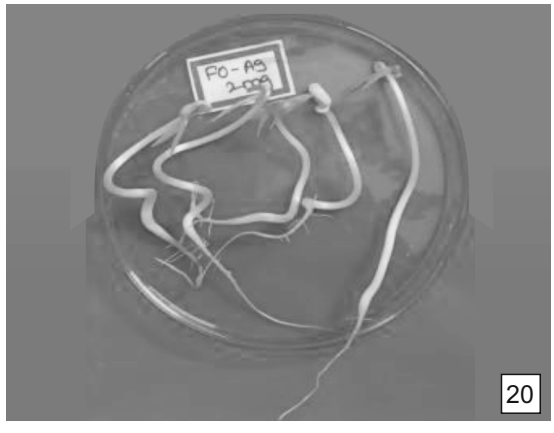

Figs 15–20: 15. TEM image of FO-AgNPs at 50 nm magnification showing the sizes of AgNPs (7–60 nm). 16. TEM image of FO-AgNPs at 20 nm magnification with clear fringes on the surface. 17. In vitro seed germination of KN AgNPs after 24 h. 18. In vitro seed germination of FO AgNPs after 24 h. 19. In vitro seed germination of KN AgNPs after 72 h. 20. In vitro seed germination of FO AgNPs after 72 h.

Figs 21 & 22: 21. In vivo seed germination activity of KN AgNPs after 35 d. 22. In vivo seed germination activity of FO AgNPs after 35 d.

TABLE 1: Germination count and germination percentage of green gram by treating with AgNPs after 24 h.

	10 ppm		20 ppm		30 ppm		40 ppm		50 ppm	
	Ger.count	Ger.%	Ger.count	Ger.%	Ger.count	Ger.%	Ger.count	Ger.%	Ger.count	Ger.%
K. nemoralis	49 ± 1	98 ± 2	48 ± 2.6	96 ± 5	46 ± 1	92 ± 2	43 ± 1.5	85 ± 3	39 ± 2.5	77 ± 5
F. ovata	47 ± 2.5	95 ± 5	49 ± 1	98 ± 2	44.3 ± 2	89 ± 4	40 ± 1	80 ± 2	36.3 ± 3	72 ± 6

Ppm, Parts per million; (Values= Mean ± Standard deviation); Ger.count, Germination count; Ger %, Germination percentage.

TABLE 2: Root and shoot lengths of green gram by treating with AgNPs after 72 h.

	10 ppm		20 ppm		30 ppm		40 ppm		50 ppm	
	RL	SL	RL	SL	RL	SL	RL	SL	RL	SL
K. nemoralis	9.4 ± 0.5	1.9 ± 0.2	7.7 ± 0.3	1.1 ± 0.2	3.6 ± 1.1	-	4.8 ± 0.8	-	1.5 ± 0.5	-
F. ovata	8.2 ± 0.8	1.4 ± 0.1	6.9 ± 0.6	1.6 ± 0.2	7.4 ± 1	0.9 ± 0.2	4.3 ± 0.5	0.6 ± 0.3	4.3 ± 0.5	0.5 ± 0.1

Ppm, Parts per million; (Values= Mean ± Standard deviation) -, Not present; RL, Root length; SL, Shoot length

TABLE 3: In vivo seedling growth observed over a period of 35 d.

In vivo seed germination for 35 d		After 7 d		After 14 d		21 d		28d		35d	
		RL	SL	RL	SL	RL	SL	RL	SL	RL	SL
K. nemoralis	10 ppm	2.1 ± 0.3	6.2 ± 0.3	4.3 ± 0.17	14.5 ± 0.3	8.3 ± 0.15	24.8 ± 0.15	8.8 ± 0.15	26.5 ± 0.26	13.8 ± 0.15	29.6 ± 0.15
	20 ppm	3.13 ± 0.2	7 ± 0.2	4.9 ± 0.36	17 ± 0.25	9.4 ± 0.26	25.5 ± 0.3	10 ± 0.15	27.5 ± 0.3	19.2 ± 0.3	31.2 ± 0.73
	30 ppm	1.86 ± 0.2	6 ± 0.25	3.6 ± 0.2	15.2 ± 0.15	6.8 ± 0.2	22.8 ± 0.11	7.1 ± 0.2	24.3 ± 0.32	15.4 ± 0.15	27.5 ± 0.37
F. ovata	10 ppm	1.16 ± 0.2	6.13 ± 0.4	2.83 ± 0.2	17.4 ± 0.32	5.86 ± 0.3	25.5 ± .36	6.4 ± 0.11	27.3 ± 0.3	15 ± 0.2	31.5 ± 0.62
	20 ppm	2.23 ± 0.3	7 ± 0.15	5.5 ± 0.34	18.3 ± 0.21	10.3 ± 0.2	27.7 ± 0.37	11 ± 0.26	32.3 ± 0.35	17.4 ± 0.15	35.3 ± 0.3
	30 ppm	1.56 ±0.21	5.86 ± 0.4	5.06 ± 0.15	15.1 ± 0.2	6.4 ± 0.26	25.4 ± 0.3	8.2 ± 0.15	26 ± 0.5	16.6 ± 0.3	28.6 ± 0.36

Ppm, Parts per million; (Values= Mean ± Standard deviation); RL, Root length; SL, Shoot length.

DISCUSSION

The reaction between $AgNO_3$ and the aqueous extracts resulted in a pronounced colour change, confirming nanoparticle synthesis and highlighting the reduction of silver ions to AgNPs. SPR peaks in the range of 427–433 nm confirm the successful formation of AgNPs, consistent with earlier reports on green synthesis using plant extracts (Huq et al. 2022, Yugandhar et al. 2015). FTIR spectra revealed the presence of functional groups like alcohols, amines and alkenes. The retained and mild shifted peaks confirm that these biomolecules not only reduce Ag^+ to Ag^0 but also stabilize the nanoparticles, preventing aggregation thus contributing to colloidal stability.

DLS reveals the smaller particles in FO- (1–9 nm, mode 1.2 nm) derived AgNPs compared to that of KN (40–70 nm, mode 49.9 nm). Smaller-sized nanoparticles are ideal for applications in photocatalysis, antimicrobial coatings, and environmental remediation (Sachin 2019). Ultra small-sized particles in FO (<10 nm) make them easily penetrate biological membranes and cross physiological barriers (e.g., blood-brain barrier), making them suitable for targeted drug delivery and tumour imaging. However, this also means that they can accumulate in sensitive organs like the kidney and brain, potentially causing toxicity (Attarilar et al. 2020). Hence, drug delivery systems through small-sized NPs require precise control and

thorough evaluation to ensure therapeutic efficacy while minimizing potential toxicity.

TEM confirmed their spherical, oval as well as irregular morphologies, while Zeta potential (–24.3mV and –18.3mV) indicate colloidal stability, aggregation tendency, and interaction potential with biological or environmental systems.

In vitro studies revealed a progressive increase in germination percentage observed with rising AgNP concentrations up to 30 ppm. Earlier studies with calcium nanoparticles also demonstrated their effect on seed germination of *Vigna* (Yugandhar & Savithramma 2013). Concentrations above 30 ppm led to a significant reduction in germination and seedling development. At 50 ppm, a lethal effect was recorded, with complete inhibition of growth, indicating that this concentration exceeds the phytotoxic threshold and causes cellular damage or metabolic disruption. Excluding the lethal concentrations above 30 ppm in vivo experiments were conducted to validate the in vitro findings, by amending soil with AgNPs and monitoring green gram growth over a 35 d period revealing the 20 ppm as optimum concentration for growth with KN-derived AgNPs resulted in the highest root length of 19.2 cm, while FO-derived AgNPs promoted the higher shoot length of 35.3 cm being noticed with observation of mild to lack of growth in conventional pests and nematodes which might be due to oxidative stress caused within the pests leading to impaired metabolism (Renu et al. 2025). The efficacy in inhibiting the growth of pests might be due to the phytometabolites and bioactive compounds like methylene bicycle (3.2.0) het-3ene2-one, trimethyl tetradecane (Bhavani et al. 2025). To establish the agronomic viability of nanoparticle treatments, comprehensive field trials and such extended investigations are required to determine whether these effects really impart their influence on flowering, pod formation, final crop yield and translate into increased yield.

The study thus demonstrated the enhanced germination and better seedling establishment after being primed with KN- and FO-derived AGNPs in dose dependent manner and above the optimum levels (~30 ppm) leading to mortality. The dual-phase response underscores the need for precise nanoparticle administration to balance efficacy and safety. Furthermore, these findings support the integration of plant-mediated nanotechnology into sustainable agriculture, while also calling for further studies to evaluate long-term yield outcomes and environmental interactions.

ACKNOWLEDGMENT

We thank Dr. V. Subbaiah, DST PURSE Centre, Sri Venkateswara University, Tirupati for his help in the characterization of synthesized nanoparticles using UV-Vis Spec, DLS, Z-potential and TEM.

Declaration

Authors' contribution

Plant collection, synthesis, experimentation and data analysis was carried out by GB and drafting and correction of the manuscript was done by NS.

Conflict of interest

Authors declare no conflict of interest.

REFERENCES

ABDELKADER M, ZARGAR M, BAYAT M, PAKINA E, SHEHATA A S A & SULIMAN A A 2024 Biogenic nano-fertilizers as a sustainable approach to alleviate nitrate accumulation and enrich quality traits of vegetable crop*s Horticulturae* **10** 789 https://doi.org/10.3390/horticulturae10080789

ABD WAHAB N Z & ABD RAHMAN A H A 2022 Phytochemical analysis and antibacterial activities of *Kyllinga nemoralis* extracts *J Pure Appl Microbiol* **16** 2568–2575 https://doi.org/10.22207/JPAM.16.4.23

ALESSANDRA FRANCINI & ANTONIO FERRANTE 2023 Advances and future propect of nitric oxide in agriculture In *Plant gasotransmitters and molecules with hormonal activity* Academic Press London pp 289–304

ALFOSEA-SIMÓN F J, BURGOS L & ALBURQUERQUE N 2025 Silver nanoparticles help plants grow alleviate stresses and fight against pathogens *Plants* **14** 428 https://doi.org/10.3390/plants14030428

ARORA P K, TRIPATHI S & OMAR R A 2024 Next-generation fertilizers: the impact of bio-nano-fertilizers on sustainable agriculture *Microbial Cell Factories* **23** 1– 18

ATTARILAR S, YANG J, EBRAHIMI M, WANG Q, LIU J, TANG Y & YANG J 2020 The toxicity phenomenon and the related occurrence in metal and metal oxide nanoparticles: A brief review from the biomedical perspective. *Front Bioeng Biotechnol* **8** 822

BHAVANI G, SAVITHRAMMA N & ANKANNA S 2025 Identification of novel bioactive compounds from *Kyllinga nemoralis Indian J Eco* **52** 505–510

CHITTORA D, PARVEEN T, YADAV J, MEENA B R, JAIN T & SHARMA K, 2023 Harmful impact of synthetic fertilizers on growing agriculture and environment *Glob J Pharmacol Pharmaceut Sci* **11** 555–804

GOYAL S, KUMAR R & BENIWAL V 2023 Biogenic synthesis of nanoparticles for sustainable crop production: A Review *Lett Appl Nano Bio Sci* **12** 10–18

HAJARE S S & AKOLE S 2022 Effect of organic and inorganic fertilizer on plant growth *World J Pharm Life Sci* **8** 101–104

HUQ M A, ASHRAFUDOULLA M, RAHMAN M M, BALUSAMY S R & AKTER S 2022 Green synthesis and potential antibacterial applications of bioactive silver nanoparticles: A Review *Polymers* **14** 742

KALE S K, PARISHWAD G V, HUSAINY A S N & PATIL A S 2021 emerging agriculture applications of silver nanoparticles *ES Food Agroforestry* **3** 17–22

PAWADE P N, CHEDE P S & KHANDEKAR U S 2018 Phytochemical analysis of leaves of *Fimbristylis ovata. IJARIIE* **4** 8936

SMPB (State Medicinal Plants Board) *Kerala Herbal Database* Retrieved October 8 2025 *Kyllinga nemoralis* –MedicinalUses https://www. smpbkerala.in/herbal-data/kyllinga-nemoralis.asp

RENU S, HANUMAN S, APEXA P, PAYAL L 2025 Ecofriendly synthesis of ZnO nanoparticles from *Calotropis procera* and their in vivo nematicidal potential *SSR Ins J Life Sci* **11** 7178–7185

SACHIN 2019 Size effects in nanomaterials: Theoretical insights *Int J Physics Appl* **1** 50–56

VENKATESWARLU P, ANKANNA S, PRASAD T N V K V, ELUMALAI E K, NAGAJYOTHI P C & SAVITHRAMMA N 2010 Green synthesis of silver nanoparticles using *Shorea tumbuggaia* stem bark *Int J Drug Dev Res* **2** 720– 723

YUGANDHAR P, HARIBABU R & SAVITHRAMMA N 2015 Synthesis characterization and antimicrobial properties of green-synthesized silver nanoparticles from stem bark extract of *Syzygium alternifolium* (Wt) Walp *Biotech* **5** 1031–1039

YUGANDHAR P & SAVITHRAMMA N 2013 Green synthesis of calcium carbonatie nanoparticles on seed germination and seedling growth of *Vigna mungo* (L) Hepper *Int J Adv Res* **1** 89–103

Journal of Cytology and Genetics 2025 VOL. **26** (NS): 73−78

RESEARCH ARTICLE

CHROMOSOMAL STUDIES ON TWO SPECIES OF *SYMPETRUM* (ODONATA: ANISOPTERA: LIBELLULIDAE) FROM HIMACHAL PRADESH

USHA KUMARI[1], MEENA KUMARI[2]* AND D. C. GAUTAM[2]

[1]Department of Zoology, Goswami Ganesh Dutt Sanatan Dharam College Rajpur, Palampur, Himachal Pradesh, 176 061, India

[2]Department of Biosciences, Himachal Pradesh University, Shimla 171 005, India

*For correspondence. Email: meenakchaudhary@gmail.com

(Received 3 October, revised accepted 26 October 2025)

SUMMARY This paper presents the chromosomal analysis of 2 species of *Sympetrum*, *Sympetrum commixtum* and *S. hypomelas* collected from Mashobra and Palampur of Himachal Pradesh respectively. The diploid chromosome number was 2n = 25 in both the species. However, they differ from each other in respect of m-chromosomes. Chromosomes were studied at mitotic and meiotic stages. Actual lengths, relative lengths and total complement lengths of chromosomes were measured at spermatogonial metaphase. Karyotypes were prepared for each species.

Keywords: *Sympetrum*, m-chromosome, total complement lengths, karyotypes.

INTRODUCTION

Order Odonata constitutes approximately 6256 species in 3 suborders Anisoptera, Zygoptera and Anisozygoptera the world over (Subramanian & Babu 2017). Family Libellulidae of suborder Anisoptera is represented by 1035 species under 144 genera. Cytogenetically, this family is well studied as compared to the other families with data available on 270 species (Walia et al. 2011). Karyological studies of family Libellulidae was done earlier by various workers (Asana & Makino 1935, Dasgupta 1957, Kiauta 1975, Sandhu & Walia 1994, Walia 2008, Walia & Sandhu 1998, 2002). The modal chromosome number of the family is 2n = 25 including a pair of m-chromosomes. Variation in chromosome number occurs due to fusion and fragmentation of holokinetic chromosomes (Agopian & Mola 1984, Kiauta 1972, Mola 1992, 1995).

Some cytogenetic features which distinguish odonates from other orders are holocentric chromosomes (Cumming 1964, Kiauta 1969a, 1969b, Nokkala et al. 2002), presence of m-chromosomes (Lefvre & McGill 1908), XX-XO type of sex determination mechanisms in most of the species (Kiauta 1969a, Peperlov & Bugrov 2001) and post-reductional meiotic division (Kiauta 1969a, 1975, Tyagi 1986).

Odonates are valuable bioindicators used to assess water quality and health of aquatic habitat. Keeping in view the importance of odonates and

lack of data on chromosomes of *S. commixtum* and *S. hypomelas* from Himachal Pradesh, the present study was undertaken.

MATERIALS AND METHODS

For chromosomal studies, adult male specimens of *S. commixtum* and *S. hypomelas* were collected from Mashobra of district Shimla and Palampur of district Kangra of Himachal Pradesh respectively.

The germinal tissue of males was dissected out in 0.9% normal saline solution. The tissue was pretreated in 0.7% sodium citrate solution for 30 min. The pretreated tissue was fixed in 1:3 acetic acid-ethanol solution for 25¬30 min at room temperature. After fixation, squashing of tissue was done in a drop of 45% acetic acid. The tissue was then pressed by putting the slides with cover slips in between the folds of blotting paper and tapped gently. Cover slips were dislodged off from the slide with a sudden jerk. The slides and cover slips were air dried for 2 or 3 d in dust free chamber.

After drying, staining was done in 2% Giemsa solution and then the slides were mounted in DPX. The permanent slides were observed under binocular research microscope and photomicrographs were taken. Well spread spermatogonial metaphase complements were selected for chromosomal measurements. Lengths of chromosomes were measured using ocular micrometer and total complement length was calculated for each species. The relative lengths were calculated from the actual length and total complement length data.

OBSERVATIONS

In the present study, the chromosomes of 2 species of dragonflies have been studied.

Sympetrum commixtum

The diploid chromosome number in this species is 25 (Fig. 1). The mean actual length of chromosomes ranges from 0.84 μm ± 0.07 S.E. (X chromosome) to 2.68 μm ± 0.08. The mean total complement length is 42.99 μm ± 0.60 S.E. The mean relative length of chromosomes ranges from 2.03 ± 0.16 S.E. (X chromosome) to 6.28 ± 0.16 S.E. (Table 1). The karyotype and idiogram show a gradual decrease in chromosome lengths (Figs 2, 3).

During pachytene, the chromosomes appear as interwoven threads (Fig. 4). At diakinesis, 13 elements are observed out of which 12 are bivalents and one X chromosome is univalent. Bivalents show rectangular shape due to the presence of interstitial chiasmata (Fig. 5). The bivalents are rod shaped at metaphase I due to condensation and X chromosome is present at the peripheral position (Fig. 6). At prophase II, autosomes show characteristic ε-shape and X chromosome appears round in form (Fig. 7).

Sympetrum hypomelas

Chromosomes are observed at spermatogonial metaphase as well as in pachytene and diakinesis. The diploid chromosome number in this species is 25 with a pair of m-chromosomes (Fig. 8). The mean actual length of chromosomes ranges from 0.58 μm ± 0.06 S.E. (m-chromosome) to 2.95 μm ± 0.07 S.E. The mean total complement length is 43.56 μm ± 0.86 S.E. The mean relative length of chromosomes

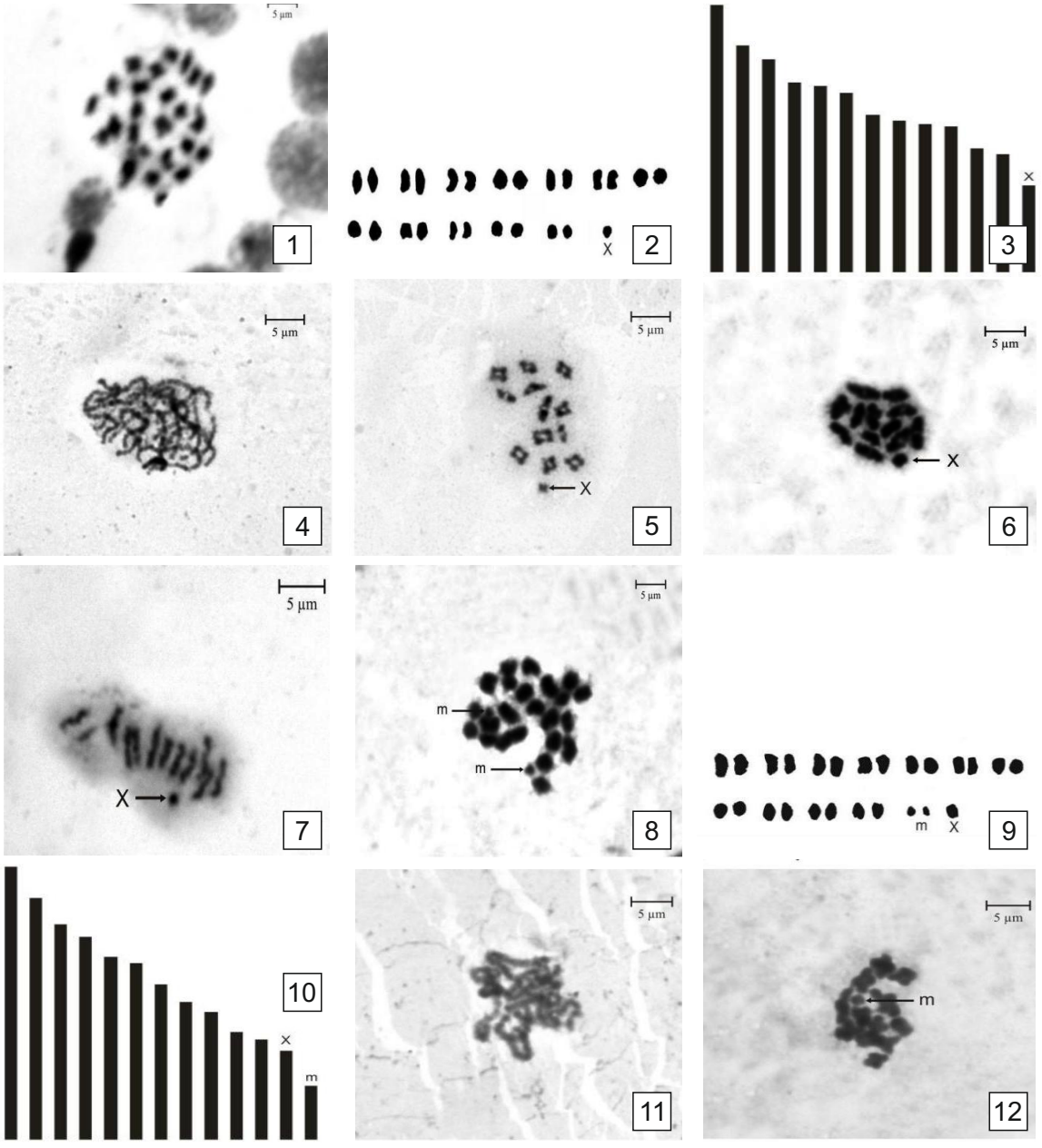

Figs 1–12: Karyotype and meiosis in *S. commixtum* and *S. hypomelas***.** 1–7. *S. commixtum.* 1. Chromosomes at spermatogonial metaphase. 2. Karyotype. 3. Idiogram. 4. Pachytene. 5. Diakinesis showing12 bivalents and univalent X-chromosome (arrow). 6. Metaphase I showing highly condensd 12 bivalents and unvalent peripheral X-chromosome (arrow). 7. Prophase II showing 12 ε-shaped chromosomes (arrow) and rounded X-chromosome. 8–12. *S. hypomelas.* 8. Chromosomes at spermatogonial metaphase.9. Karyotype. 10. Idiogram. 11. Pachytene. 12. Diakinesis showing 13 elements including smallest m-chromosome (arrow).

TABLE 1: Mean actual length, mean relative length and total complement length at spermatogonial metaphase.

Chromosome pair	Mean actual length (μm) .		Mean relative length	
	S.commixtum	*S. hypomelas*	*S. commixtum*	*S. hypomelas*
1	2.68 ±0.08	6.28± 0.16	2.95± 0.07	6.75± 0.10
2	2.27 ±0.05	5.33± 0.09	2.61± 0.07	6.00± 0.14
3	2.14 ±0.05	4.98± 0.09	2.32± 0.03	5.33± 0.08
4	1.96 ±0.05	4.46± 0.07	2.18± 0.03	5.02± 0.10
5	1.88 ±0.02	4.38± 0.04	1.97± 0.05	4.53± 0.06
6	1.81 ±0.03	4.21± 0.06	1.90± 0.04	4.36± 0.07
7	1.62 ±0.06	3.68± 0.10	1.68± 0.06	3.84± 0.08
8	1.53 ±0.02	3.56± 0.05	1.49± 0.05	3.42± 0.07
9	1.49 ±0.00	3.47± 0.05	1.38± 0.06	3.16± 0.09
10	1.47 ±0.02	3.43± 0.06	1.16± 0.04	2.66± 0.06
11	1.23 ±0.06	2.90± 0.12	1.08± 0.04	2.49± 0.07
12	1.02 ±0.06	2.46± 0.14	0.58**± 0.06	1.32**± 0.13
X Chromosome	0.82* ±0.07	1.99*± 0.18	0.97*± 0.08	2.21*± 0.18
Total complement length	43.02 ± 0.58		43.56 ± 0.86	

**For m-chromosome; *For X chromosome.

ranges from 1.32 ± 0.13 S.E. (m- chromosome) to 6.76 ± 0.10 S.E. The mean actual length and mean relative length of X chromosome were 0.97 µm ± 0.08 S.E. and 2.21 ± 0.18 S.E. respectively (Table 1). The karyotype and the idiogram show a gradual decrease in chromosome lengths with m-chromosome pair being the smallest pair of the complement (Figs 9, 10).

During pachytene, the chromosomes become more distinct in the form of a network (Fig. 11). At diakinesis, chromosomes appear more condensed and 13 elements are visible. These included 12 autosomal bivalents and one sex univalent. Autosomes appear cross-shaped due to the presence of interstitial chiasmata (Fig. 12).

DISCUSSION

Karyotypes of about 607 species (198 genera, 23 families) of odonates covering approximately 10% of described species are known. Most of the cytogenetic data pertain to family Libellulidae as compared to other families. 39 species belonging to this family are karyologically described from India till date (Kuznetsova & Golub, 2020). In the 2 species of the family Libellulidae studied here, S. *commixtum* have diploid chromosome number of 25. The m-chromosome pair was lacking in this species. Similar findings were earlier reported by Tyagi (1978). This chromosome number was in agreement with modal number of the family i.e., 2n = 25 but deviates from it in the absence of m-chromosome pair. The diploid chromosome number in *S. hypomelas* was found to be 25. This was the first chromosome number report for this species. This chromosome number was in agreement with the type number of 2n = 25 including a pair of m-chromosomes of the family.

Present studies are suggestive of diffused nature of centromere and XO type of sex determination system in both the species. However, rectangular shaped bivalents are due to presence of interstitial chiasmata. Univalent X chromosome divides post-reductionally. These investigations are in conformity with the findings of earlier workers on other odonate species (Handa et al. 1984, Kiauta 1967, 1969a, 1969b, 1975, Tyagi 1978).

ACKNOWLEDGEMENT

Usha Kumari gratefully acknowledges the financial assistance provided by UGC-BSR fellowship to complete this work successfully.

Authors' contribution

UK carried out the research work and prepared the manuscript. MK edited and drafted it. DCG guided and mentored this work.

Conflict of interest

All authors have no conflict of interest.

REFERENCES

AGOPIAN S S & MOLA L M 1984 Bandeo C en Odonata *Abstr Pap XV Congr Soc Arg deGenetica Corrientes* pp 17

ASANA J J & MAKINO S 1935 A comparative study of the chromosomes in the Indian dragonflies *J Fac Sci Hokkaido Imp Univ Ser VI* **4** 67-–86

CUMMING R B 1964 *Cytogenetic studies in order Odonata* Ph D Thesis University of Texas

DASGUPTA J 1957 Cytological studies of some Indian dragonflies II A study of the chromosomes during meiosis in thirty species of Indian Odonata (Insecta) *Proc Zool Soc Calcutta* **10** 1–65

HANDA S M, MITTAL O P & BATRA H N 1984 Chromosomes in ten species of dragonflies (Anisoptera: Odonata) *Res Bull Punjab Univ* **35** 65–73

KIAUTA B 1967 Considerations on the evolution of chromosome complement in Odonata *Genetica* **38** 430–446

KIAUTA B 1969a Sex chromosomes and sex determining mechanisms in Odonata with a review of the cytological conditions in the family Gomphidae and references to the karyotypic evolution in the order *Genetica* **40** 127–157

KIAUTA B 1969b Autosomal fragmentations and fusions in Odonata and their evolutionary implications *Genetica* **40** 158–180

KIAUTA B 1972 Synopsis on the main cytotaxonomic data in the order Odonata *Odonatologica* **1** 73–102

KIAUTA B 1975 *Cytotaxonomy of dragonflies with special reference to the Nepalese fauna* Nepal Research Centre Kathmandu

KUZNETSOVA V G & GOLUB N 2020 A checklist of chromosome numbers and a review of karyotype variation in Odonata of the world *Comp Cytogenet* **14** 501–540

LEFEVRE G & MCGILL C 1908 The chromosomes of *Anasa tristis* and *Anax junius Amer J Anat* **7** 467–487

MOLA L M 1992 *Estudios cromosomicos en libelulas (Orden Odonata)* Tesis de Doctorado Facultad de Ciencias Exact y Natural Universidad Buenos Aires pp187

MOLA L M 1995 Post-reductional meiosis in *Aeshna* (Aeshnidae Odonata) *Hereditas* **122** 47–55

NOKKALA S, LAUKKANEN A & NOKKALA C 2002 Mitotic and meiotic chromosomes in *Somatochlora metallica* (Cordulidae Odonata) The absence of localized centromeres and inverted meiosis *Hereditas* **136** 7–12

PEREPELOV E & BUGROV A G 2001 C-heterochromatin in chromosomes of *Ophiogomphus cecilia cecilia* (Four) (Anisoptera: Gomphidae) with notes on the sex chromosome origin in the species *Caryologia* **54** 169–172

SANDHU R & WALIA G K 1994 Karyological study on four female libellulids from Assam (India) *Fraseria* **1** 11–14

SUBRAMANIAN K A & BABU R 2017 *A Checklist of Odonata (Insecta) of India* Version 3 Zoological Survey of India Kolkata

TYAGI B K 1978 The chromosome numbers and sex-determining mechanisms newly recorded in thirteen Indian dragonflies (Odonata) *Chrom Inf Serv* **25** 5–7

TYAGI B K 1986 Cytogenetics karyosystematics and cytophylogeny of Indian Odonata *Indian Rev Life Sci* **6** 221–239

WALIA G K 2008 Comparative cytological data on twentysix species of family Libellulidae (Anisoptera: Odonata) *Fraseria* **7** 77–82

WALIA G K & SANDHU R 1998 Female karyotypic study of four species of family Libellulidae (Anisoptera: Odonata) *Fraseria* **5** 63–67

WALIA G K & SANDHU R 2002 Chromosomal data on seven species of genus *Orthetrum* (Libellulidae: Anisoptera: Odonata) *Bionature* **22** 7–12

WALIA G K, KAUR H & KAUR J 2011 Karyotypic variations in the chromosome complement of *Pantala flavescens* (Fabricius) of the family Libellulidae (Anisoptera: Odonata) *Cytologia* **76** 301–307